공학박사학위논문

공기열원 열펌프의 냉매누설량 탐지방법에 대한 연구

Study on the Detection Method of Refrigerant Leakage Amount in Air Heat Pump System

2018 년 2 월

서울대학교 대학원

기계항공공학부

류 진 우

공기열원 열펌프의 냉매누설량 탐지방법에 대한 연구

Study on the Detection Method of Refrigerant Leakage Amount in Air Heat Pump System

지도교수 김 민 수

이 논문을 공학박사 학위논문으로 제출함

2017 년 10 월

서울대학교 대학원

기계항공공학부

류 진 우

류진우의 공학박사 학위논문을 인준함

2017 년 12 월

위 원 장 : 민 경 덕

부위원장 : 김 민 수

위 원 : 송 한 호

위 원 : 도 형 록

위 원 : 장 영 수

Abstract

Study on the Detection Method of Refrigerant Leakage Amount in Air Heat Pump System

Jin Woo Yoo

Department of Mechanical and Aerospace Engineering

The Graduate School

Seoul National University

In this study, the two detection methods of refrigerant leakage amount in air heat pump systems are suggested and verified by modeling and experiment. This is important because one of the most frequently occurred and the most costly fault in heat pumps is refrigerant leakage. When a leak occurs, the leak point needs to be found and it is relatively easy once we have proper leak detector. After that, charge amount leaked from the system needs to be determined by the system behavior and to be recovered.

The modeling process of the heat pump system requires lubricant consideration because the optimal charge amount in the modeling without

lubricant is largely underpredicted compare with experimental results. This difference is mainly due to the refrigerant amount dissolved in the lubricant. The effect of heat transfer and pressure drop from the lubricant is relatively small but the refrigerant dissolves in the oil as a form of the liquid, which makes its amount large significantly. When the lubricant is considered in the modeling, the results show good matches with experiment.

With the modeling and the experiment from two different heat pump systems, which are the residential and commercial type, the refrigerant detection method is suggested. The residential system only has a small number of sensors and within this limitation, the current charge amount needs to be found. The method utilizes the temperature sensor at evaporator side, which are located at the indoor air inlet and evaporator midpoint. The temperature difference between these two is a detection judgment index. It is larger than the 5K at normal charge condition because evaporator midpoint stays at the two-phase condition. At leaked condition, the evaporator midpoint state becomes superheated so the temperature difference at evaporator becomes smaller than 5K. With this principle, charge level around 55 to 65% is judged. Additionally with the EEV control method, which intentionally reduces the opening value of EEV, the detection range of charge level increases to 80%.

For commercial type, the detection method with log mean temperature

difference (LMTD) at condenser is suggested. This is because the relationship between the charge level and condensing pressure showed linearity. The data divided into groups according to the compressor rotational speed. With the compensated LMTD at condenser charge amount in the system is predicted with RMS error of 5.9%.

This study is useful for any air heat pump system and the proposed methods can be applied immediately to existing systems.

Keyword: Air heat pump, Lubricant and refrigerant mixture, Refrigerant charge amount, Leakage amount detection

***Identification Number*: 2012-22555**

Contents

List of Figure

List of Tables

Nomenclature

A	area (m^2)
Bo	Boiling number
C	clearance volume ratio, constants
C_d	drag coefficient
C_p	specific heat (kJ/kg·K)
COP	coefficient of performance
DSC	degree of subcool (K)
DSH	degree of superheat (K)
d	diameter (m)
d_c	fin collar outside diameter (m)
d_h	hydraulic diameter (m)
E	enhancement factor
EEV	electronic expansion valve
F_p	fin pitch (m)
f	friction factor
G	mass flux ($kg/s \cdot m^2$)
g	gravitational accerleration (= 9.81 m/s^2)
h	heat transfer coefficient ($kW/m^2 \cdot K$)
i	enthalpy (kJ/kg)
j	Couburn j factor
k	thermal conductivity (kW/m·K)

L	depth of the heat exchanger in air flow direction, length of pipe (m)
LMTD	log mean temperature difference (˚C)
m	mass (kg)
$\dot{m}$	mass flow rate (kg/s)
N	number of tube rows
Nu	Nusselt number
n	polytropic coefficient
OCR	oil circulation ratio
P	pressure (kPa)
p_l	longitudinal tube pitch (m)
p_t	traverse tube pitch (m)
Pr	Prandtl number
Q	cooling or heating capacity (kW)
q	vapor quality
q''	heat flux (kW/m^2)
Re	Reynolds number
R,r	radius (m)
T	temperature (K)
u	uncertainty
U	overall heat transfer coefficient ($kW/m^2 \cdot K$)
V	volume (m^3)
$\dot{V}$	volume flow rate (m^3/s)
v	velocity (m/s)
W	compressor work (kW)

w	solubility (the mass ratio of liquid refrigerant to liquid mixture of oil and refrigerant)
z	liquid fraction in total mixture or length in z-direction (m)

Greek

α_{VF}	void fraction
δ	thicness of fin or liquid film (m)
ε	roughness (m)
ρ	density (kg/m^3)
ν	kinematic viscosity (mm^2/s)
η	efficiency
ω	compressor rotational speed (Hz)
μ	dynamic viscisity (Pa·s)
τ	shear stress (kPa)

Subscript

air	air side
comp	compressor
d	dischrage
disp	displacement
EEV	electronic expansion valve
f	fin side

g	gas phase
i	inner
in	inlet
l,liq	liquid
lo	liquid only
max	maximum
mix	mixture
o	outer
oil	oil or lubricant
out	outlet
ref	refrigerant side
s	suction
tp	two-phase
vap	vapor
wall	tube wall side

Chapter 1. Introduction

1.1 Background of the study

HVAC (Heating, Ventilation & Air Conditioning) is a technology that provides human thermal comfort and quality air. It always exists where people live because finding comfort zone is a basic human instinct. Without a doubt, the energy use through HVAC is extremely large. In the United States, HVAC takes 40% of residential, building and commercial energy use (2011 Buildings Energy Data Book) and heat pumps play an essential role in it. From the researches of Biddle (2008) and U.S. Energy Information Administration (2012), the penetration rate of the heat pump in the United State over time is presented in Fig. 1.1. Residential heat pump first led the market as a form of air-conditioner but commercial heat pump become popular these days. The market for both residential and commercial heat pump systems continue to increase. Due to the high penetration rate of heat pump the maintenance of it is important.

One of the most frequently occurred and costly fault in heat pumps is refrigerant leakage. In fact, the system using refrigeration cycle have the same problem. In Fig. 1.2, Comstock and Braun (1999), Rossi (2004), Madani and

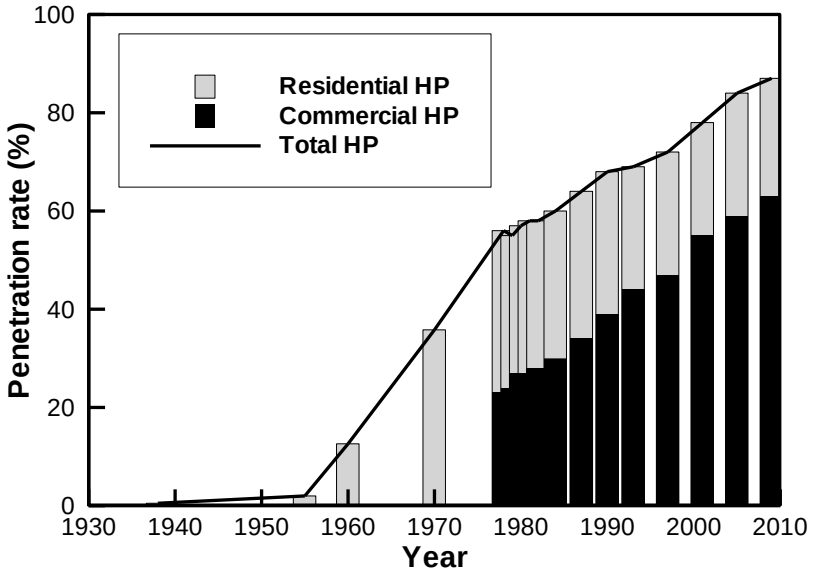

Fig. 1.1 The penetration rate of Heat pump(air conditioner) in the United State

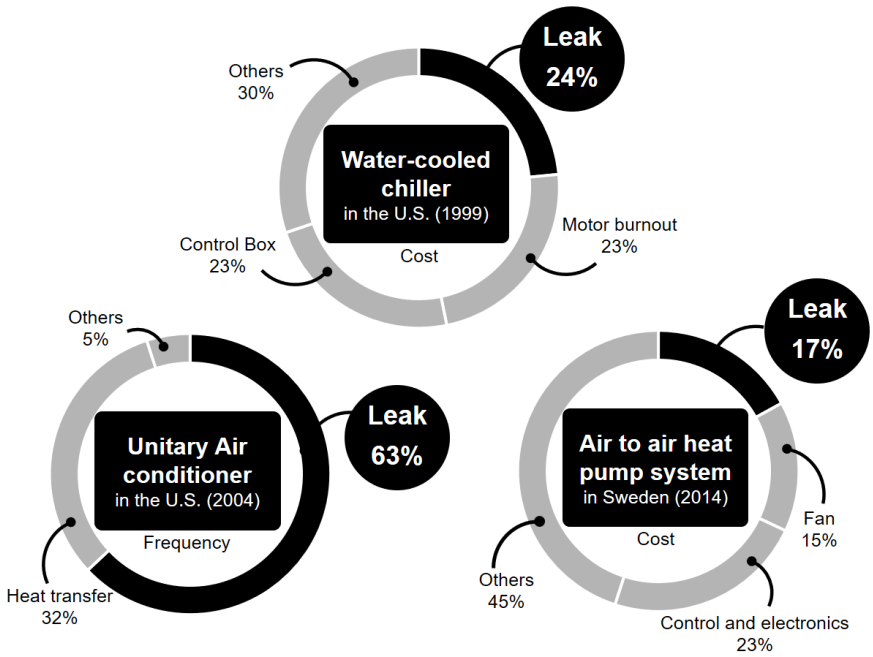

Fig. 1.2 Cost (or frequency) of faults in the systems using heat pump cycle

Roccatello (2014) showed the types of faults and cost (or frequency) from it in water chiller, air-conditioner, and heat pump, respectively. In these research papers, refrigerant leakage occupies large portion and it becomes the first problem if electrical problems are not concerned. Mowris et al. (2004) even insisted that 72% of air conditioners have improper charge amount. Leaked refrigerants elevate global warming effect and harm people with its toxicity. Therefore, detecting the refrigerant leakage is necessary. Refrigerant leakage not only has environmental harm but also significantly degrade system performance. All the heat pump systems have its optimal refrigerant charge amount that maximizes the coefficient of performance (COP). Fig. 1.3 shows the COP variation with respect to refrigerant charge amount in a water heat pump. (Corberán et al., 2008) The performance of heat pump decreases noticeably at non-optimum refrigerant charge amount. Similar results are found from previous studies. (Corberán et al., 2011; Grill and Singh, 2017; Kim et al., 2007; Kim et al., 2014; Kim, 2017; Yoo et al., 2017) From two facts that refrigerant leakage has a harmful effect and degrades system performance when the leak occurs, two actions need to be taken. The first action is to find leak point and fix it. The location of refrigerant leakage can be easily detected once we have a proper refrigerant detector. The types of refrigerant detector are shown in Fig. 1.4 and fluorescent leak detector and electronic detectors can also

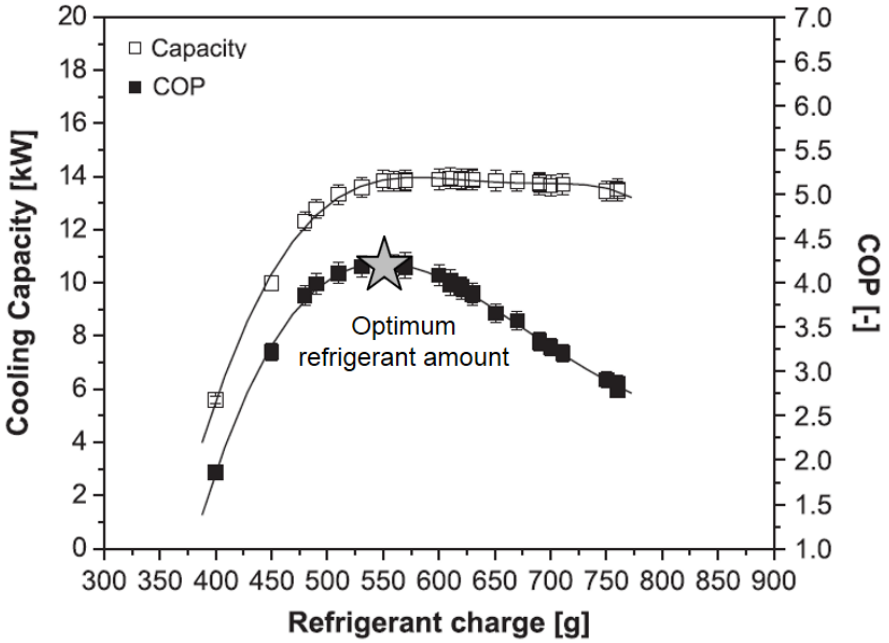

Fig. 1.3 COP and cooling capacity with respect to refrigerant charge amount (Corberán et al., 2008)

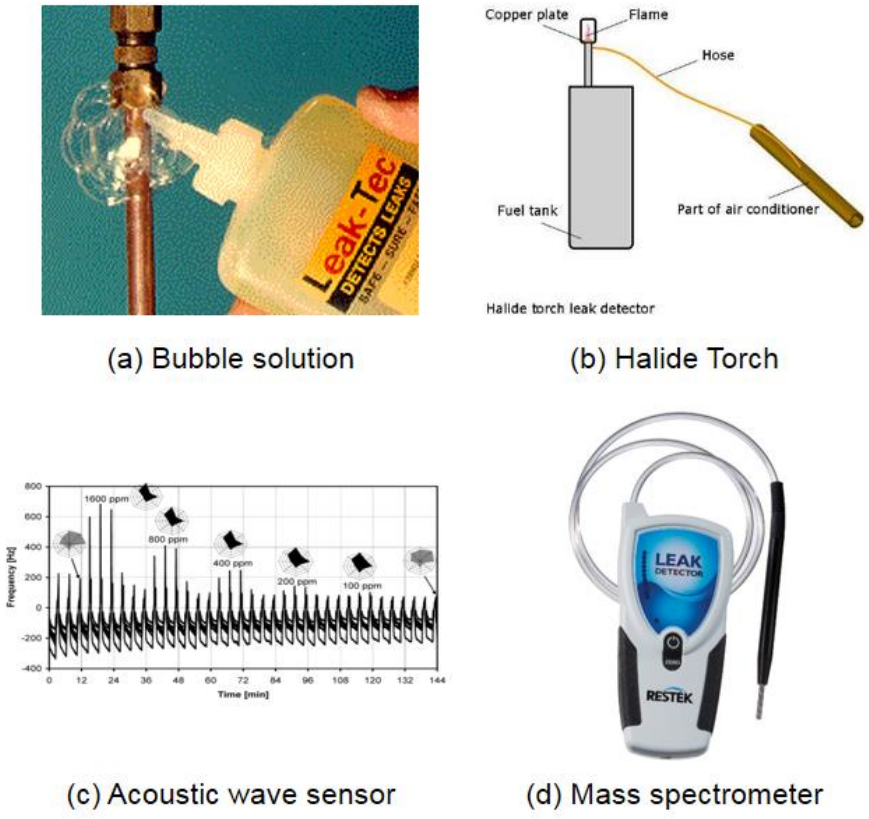

Fig. 1.4 Types of refrigerant detector

be used. The second action is to recover refrigerant charge. Before the recovery process of refrigerant in heat pump system, the amount of leaked refrigerant need to be determined but it is not easy to quantify it from the system behavior.

The simplest method for refrigerant leakage detection that anyone can think is to measure the pressure and temperature of the system when it is stopped. Fig. 1.5 shows pressure variation at different refrigerant charge amount in one of the commercial heat pump system when air temperature condition is fixed. The optimal charge amount for this system is 9 kg. When the charge amount drops to half (4.5 kg) the pressure is only reduced by 10%. This means it is hard to quantify current charge amount when the system is not operating unless the charge amount is significantly low. For this reason, it needs to be determined when the system is in operation.

The type of air heat pump can be divided into two groups, which are the residential and commercial type, and they have several different features. The residential heat pump usually has single outdoor and single indoor unit while the commercial heat pump have multiple outdoor and indoor units. The capacity ranges are around 2~11 kW for residential heat pump and 20~300 kW for commercial heat pump. Residential air heat pump has a low number of part and joints and the system is relatively simple. However, only a small number of sensors are installed in the system because of cost reduction. On the other hand,

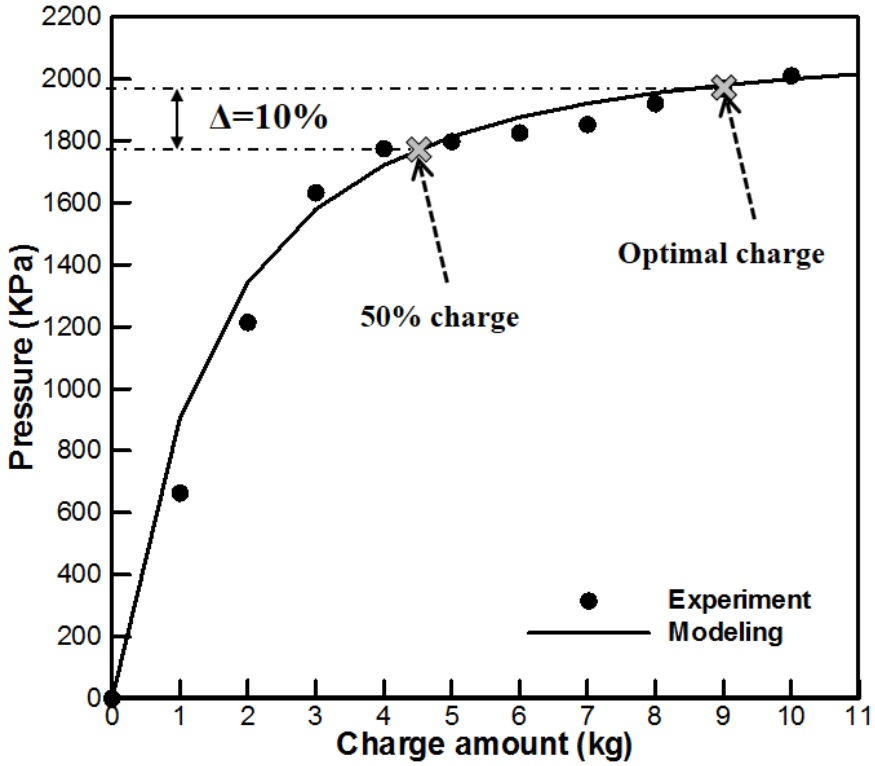

Fig. 1.5 Refrigerant charge amount vs. pressure (Non-operating condition at

T_{indoor} = 27°C, $T_{outdoor}$ = 35°C)

commercial air heat pump relatively has various sensor information but it usually is a complex system with many parts and joints. Both systems require refrigerant detection but the target is somewhat different. For residential heat pump system, it needs to be done with the smallest possible number of the sensor. For commercial heat pump system, the level of accuracy and sensitivity are more important. In this study, the method to determine refrigerant leakage amount is suggested and it is verified with modeling and experiment.

1.2 Literature survey

1.2.1 Lubricant and refrigerant mixtures for heat pump modeling

In order to set and verify the method for refrigerant leakage amount detection, both modeling and experiment are required. In the modeling process, the type and amount of lubricant is a crucial factor in the heat pump systems, especially when calculating charge amount. A lubricant of heat pump system is usually oil, so the terms 'lubricant' and 'oil' have the same meaning in this study. Oil of heat pump is selected according to the type of refrigerant. The main role of oil is to lubricate the surface between contacting metal part of the compressor. After lubrication, some of the lubricants migrates in the system and it needs to be returned to the compressor in order to maintain the lubrication process. To make the refrigerant return back to compressor lubricant and refrigerant should be mixed. This is because oil itself usually has a high viscosity so by mixing with refrigerant oil return process is much smoother. (ASHRAE Handbook, 2014)

The ratio and amount of refrigerant dissolved in the mixture vary with lubricant type and amount. Martı´nez-Galva´n et al. (2011) conducted an experiment and showed the oil type influence on the optimal charge in a

propane chiller. The optimal charge amount of system is increased from 479 to 539 g when lubricant is changed from polyolester (POE) oil to mineral oil, which is 12% difference. This is due to the difference in solubility between each oil and propane. The refrigerant dissolves in the lubricant as a form of liquid. For this reason, the amount of refrigerant dissolved in the lubricant is never negligible Peuker (2010) measured the refrigerant mass of each component in a heat pump system and showed the accumulator has a sizable amount of refrigerant. The original role of the accumulator is to prevent the possibility of liquid entrainment into the compressor during start-up. When the system reaches the steady-state condition, its state becomes a superheated state. Theoretically, it becomes gas-phase, thereby the amount of refrigerant should be very small. However, Peuker also measured the mass of lubricant and almost half of the lubricant was found in the accumulator. Jin and Hrnjak (2016) also showed that refrigerant amount change with respect to oil circulation ratio (OCR). From this, it can be easily guessed that the lubricant is the main factor to find out the exact amount refrigerant in the system. Since lubricant is basically everywhere in the system, the amount of refrigerant and lubricant needs to be calculated simultaneously in the modeling.

1.2.2 The detection method of refrigerant leakage amount

Most research papers for the detection method of refrigerant leakage amount utilized the degree of superheat (DSH) at the compressor inlet and degree of subcool (DSC) at condenser outlet as judgement value. Rossi and Braun (1997) used fault diagnostic classification method and found out that DSH and DSC is the most dominant factor to judge refrigerant leak. Grace et al. (2005) and Tassou and Grace (2005) also emphasized the importance of DSH and DSC. At undercharge condition, DSH needs to be monitored but at overcharge condition, DSC should be checked. Kim and Kim (2005) showed a gradual decrease of DSC as leakage portion increases. The result of Kocyigit's work (2014) also implies the importance of DSH and DSC. However, aforementioned research papers only suggested the sensitive parameters (DSH and DSC) of refrigerant charge amount but did not provide any specific method to find the level of charge in the system.

Li and Braun (2007, 2009) proposed virtual refrigerant charge sensor (VRC), which is based on the change in DSH and DSC. They assumed that the DSH and DSC values are coupled parameter and showed the change of each parameter have a specific ratio. Based on this method, consecutive studies were done. Kim and Braun (2013) verified this method with the system that has an accumulator. Furthermore, Kim and Braun (2015) modified this model to use it

to the system with variable speed compressor. Quality of evaporator inlet and DSH at compressor discharge were added as a parameter of VRC. Li et al. (2016) and Liu et al. (2017) made progress on this method with the data-based method and principal component analysis (PCA), respectively. Up to now, the most popular method from the literature for refrigerant leakage amount detection is VRC. However, this method is limited to fixed orifice expansion device or thermal expansion valves (TXV) that flow area at expansion device is fixed or in a small range. These days, most heat pump system have electronic expansion valve (EEV) which actively control the flow area and VRC no longer suitable. Besides, some of the developed methods (data-based and PCA) are limited to specific system and not directly applicable to any system and requires complex data processing. Therefore, to overcome this limitation new method for refrigerant leak amount detection method is required.

1.3 Objectives and scopes

The requirement for refrigerant leakage amount detection in residential and commercial heat pump system is different. For residential system, the number and cost of sensors in the system need to be minimized. For commercial system, the detection method with high accuracy and sensitivity is required. The objective of this study is to find the methods for refrigerant leakage amount detection, which are suitable for residential and commercial air heat pump. In order to propose and verify these methods, modeling and experiment are done.

In chapter 2, modeling of air heat pump system with lubricant is presented. The necessity of refrigerant and lubricant mixture calculation is explained. The properties of mixture such is treated and a detail process of heat pump modeling for both residential and commercial type heat pump is introduced.

In chapter 3, the refrigerant leakage amount judgement for residential type is proposed. The method is the simple and suitable for the system with electronic expansion valve (EEV). It is based on the temperature difference between air inlet and heat exchanger midpoint. The principle of this method is explained and verified with both modeling and experiment.

In chapter 4, the detection method for commercial type is suggested. The importance of the condenser for charge detection is explained. Then the method is suggested and it is based on the log mean temperature difference at the

condenser.

In the last chapter, a brief summary of the study and conclusion are given.

Chapter 2. Modeling of air heat pump system with lubricant

2.1 Introduction

This chapter describes the steady state modeling procedures for residential and commercial air heat pump systems with refrigerant charge amount. The amount of refrigerant calculated from the modeling is usually underestimated when compared with the experimental results. Figs. 2.1 and 2.2 show the COP change for the refrigerant charge amount of the residential and commercial air heat pump, respectively, in the experiment and modeling. The air inlet temperature of indoor side is 27˚C and that of outdoor side is 35˚C. The optimal amount of charge is defined at the point where COP is maximized and is different for experiment and modeling. For the residential system, it is 900 g in the experiment and 700 g in the modeling. Similarly, for the commercial system, it is 9 kg in the experiment and 8 kg in the modeling. The charge amount difference in percentage in the residential and commercial system between modeling and experiment by 22% and 11%, respectively. It is clear that the optimal amount of charge obtained from modeling is less than the experiment

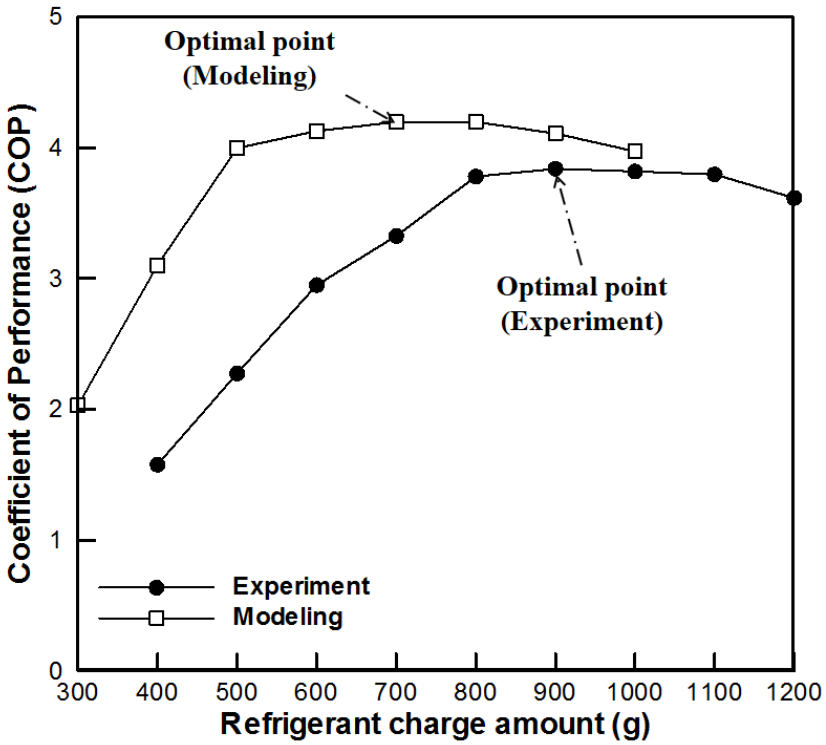

Fig. 2.1 Refrigerant charge amount versus coefficient of performance in experiment and modeling (residential heat pump)

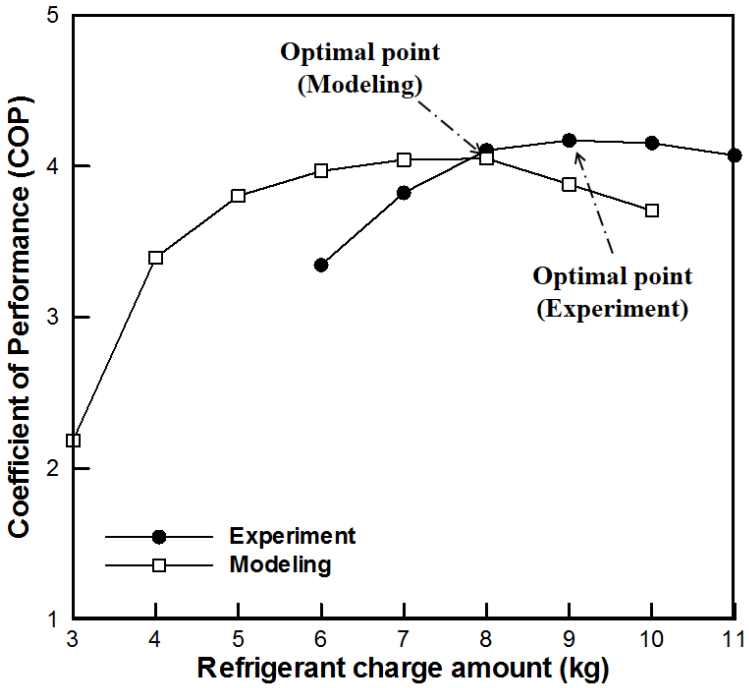

Fig. 2.2 Refrigerant charge amount versus coefficient of performance in experiment and modeling (commercial heat pump)

value.

This difference is mainly due to the two factors. One of them is the lubricant. Normally, heat pump system modeling is done without lubricant because the oil circulation ratio is generally small (less than 5%) so the effect of oil on heat transfer and pressure drop is negligible. (Shen and Groll, 2005a; 2005b) However, the effect of lubricating oil on the amount of refrigerant charge in the heat pump system is significant. The refrigerant is dissolved in the oil in liquid form and the amount of refrigerant in the mixture is not negligible. Therefore, the properties of the mixture, such as solubility, viscosity, and enthalpy, are required in order to calculate the correct amount of refrigerant charge in the system. Otherwise ,the amount will always be underestimated.

The other factor is the flow path or flow distribution. When the refrigerant flow is divided into multiple flows, the most efficient way is to have the same mass flow rate for every branching tube. Thereby, in the modeling, it is assumed that the mass flow rate is evenly distributed. However, if the flow at each branch is not the same, liquid accumulates at the bottom of the heat exchanger, increasing the charge of refrigerant in the system during the experiment. In the study by Peuker (2010), the difference in charge amount between modeling and experiment due this uneven distribution factor is about 5% in the microchannel heat exchanger.

Between the two factors, the lubricant is much more dominant. As seen in Figs 2.1 and 2.2, the uneven distribution cannot fully explain the difference between the optimal charge amount of refrigerant in the experiment and modeling. Therefore, the lubricant is mostly considered in this chapter.

2.2 Properties of lubricant and refrigerant mixture

For both residential and commercial type air heat pump system, R410A and FVC68D (polyvinyl ether: PVE) are used as a refrigerant and a lubricant, respectively. The graphs of mixture property (solubility, viscosity and enthalpy) were acquired from the manufacturer. With the given data, equations of mixture properties were derived. Solubility, viscosity and enthalpy equations were obtained according to Hewitt et al. (1991), ASHRAE handbook (2014) and Hughes (1982), respectively.

Solubility equation:

$$\log_{10} P = C_0 + C_1 w^{-0.5} + C_2 T^{-1} + C_3 w^{-0.5} T^{-1} + C_4 w^2 (T - 273.15) + C_5 w (T - 273.15) + C_6 (T - 273.15) \quad (2.1)$$

Viscosity equation:

$$\log\log(\nu + f(\nu)) = A + B\log(T) \quad (2.2)$$

Enthalpy equation:

$$i_{mix} = (1 - z) \cdot i_{ref,vap} + z \cdot w \cdot i_{ref,liq} + z \cdot (1 - w) \cdot i_{ref,liq} \quad (2.3)$$

Pure refrigerant properties are obtained from REFPROP 9.1. The phase of

pure refrigerant is classified into three, which is superheated, subcooled and two-phase states. On the other hand, the state of the lubricant and refrigerant mixture is divided into two. One is a subcooled state where both refrigerant and oil are liquid. The other is a combined state (superheated and two-phase) consisting of liquid and vapor refrigerant and liquid oil. Usually, the number of mixture states is greater than that of pure states. However, in this case, it is smaller because the vapor state of the lubricant is not taken into account. The vapor pressure of the lubricant is too low that oil is assumed to exist in only in liquid phase.

2.3 Component modeling

2.3.1 Compressor and electronic expansion valve (EEV)

The type of compressor depends on the capacity of the system. For residential heat pumps, rotary vane type compressors are used; for commercial heat pumps, scroll compressors are applied. Since both types are classified as volume displacement compressors, the modeling procedure is the same. In compressor modeling, the pressure and temperature at the compressor inlet, and the pressure at the compressor outlet are assumed. Compressor outlet temperature, refrigerant flow rate and compressor power consumption are calculated from modeling. Assuming polytropic changes during compression, the temperature at the compressor outlet is obtained from Eq. (2.4).

$$T_d = T_s(P_s/P_d)^{\frac{1-n}{n}} \tag{2.4}$$

The polytropic coefficient (n) is obtained empirically. During compression, not all refrigerant from the inlet side exits the compressor. Volumetric type compressors have a clearance volume and cause re-expansion, which reduces the mass flow of the compressor compared to the theoretical one. Volumetric

efficiency in Eq. (2.5) is defined as the ratio between the volumetric flow rate leaving the compressor and the compressor displacement rate.

$$\eta_V = 1 - C\left(\frac{\rho_d}{\rho_s} - 1\right) \tag{2.5}$$

The clearance volume ratio (C) is defined empirically. The compressors in the systems are the variable-speed type and the mass flow rate is expressed by Eq. (2.6).

$$\dot{m}_{comp} = \eta_V \rho_s V_{disp} \omega \tag{2.6}$$

From the state of the compressor inlet and outlet, and the mass flow rate of refrigerant from the compressor, the power used by compressor is obtained with Eq. (2.7).

$$W_{comp} = \dot{m}_{comp}(i_d - i_s) \tag{2.7}$$

An expansion device is one of the essential components of a heat pump that maintains the pressure difference in the system and controls the mass flow rate of the system. For electronic expansion valve (EEV) model, simple orifice

equation in Eq. (2.8) is used and drag coefficient (C_d) is determined experimentally.

$$\dot{m}_{EEV} = C_d A_{EEV} \sqrt{2\rho_{EEV,in}(P_{EEV,in} - P_{EEV,out})} \quad (2.8)$$

The area of the EEV is determined by the opening of the valve. The enthalpy values are assumed to be the same at the inlet and outlet of the EEV.

2.3.2 Condenser and evaporator - Heat transfer, pressure drop, charge amount and flow path

The air heat pump uses a fin-tube type heat exchanger as condenser and evaporator. Through the finite volume method, the heat transfer rate, pressure drop and charge amount of refrigerant and lubricant for a single grid volume are calculated. A flow path with the geometry of the heat exchanger is also considered in the modeling.

Under steady-state conditions, the overall heat transfer coefficient (U) is calculated according to Eq. (2.9). (Wang and Chi, 2000)

$$\frac{1}{UA} = \frac{1}{\eta_{air} h_{air} A_{air}} + \frac{1}{2} \ln\left(\frac{d_o}{d_i}\right) \frac{d_o}{k_{wall} A_{wall}} + \frac{1}{h_{ref} A_{ref}} \quad (2.9)$$

The effectiveness-NTU (number of transfer unit) method is applied to calculate the heat transfer between air and refrigerant.

The heat transfer coefficient of air side (h_{air}) is obtained from the Couburn j factor of Eq. (2.10). Couburn j factor is acquired from Eq. (2.11-16) and is related to the geometry of heat exchangers and air flow conditions. (Wang et al., 2000)

$$j = \frac{h_{air}}{\rho_{air} V_{max} C_{p,air}} \mathrm{Pr}^{2/3} \quad (2.10)$$

$$j = 0.086 \mathrm{Re}_{d_c}^{c1} N^{c2} \left(\frac{F_p}{d_c}\right)^{c3} \left(\frac{F_p}{d_h}\right)^{c4} \left(\frac{F_p}{p_t}\right)^{-0.93} \quad (2.11)$$

$$c1 = -0.361 - \frac{0.042N}{\ln Re_{d_c}} + 0.158 \ln\left(N \left(\frac{F_p}{d_c}\right)^{0.41}\right) \quad (2.12)$$

$$c2 = -1.224 - \frac{0.076N\left(\frac{p_l}{d_h}\right)^{1.42}}{\ln Re_{d_c}} \quad (2.13)$$

$$c3 = -0.083 + \frac{0.058N}{\ln Re_{d_c}} \quad (2.14)$$

$$c4 = -5.735 + 1.21 \ln\left(\frac{Re_{d_c}}{N}\right) \quad (2.15)$$

$$D_h = \frac{4A_c L}{A_o} \quad (2.16)$$

The surface efficiency (η_{air}) is defined as Eqs. (2.17-19)

$$\eta_{air} = 1 - \left(\frac{A_o}{A_i}\right)(1 - \eta) \tag{2.17}$$

$$\eta = \frac{\tanh(Mr\phi)}{Mr\phi} \tag{2.18}$$

$$M = \sqrt{\frac{2h_{air}}{k_f \delta_f}} \tag{2.19}$$

Where M and Φ are acquired from geometry and air flow conditions. The heat transfer coefficient on the refrigerant side (h_{ref}) is calculated according to its state. When the refrigerant is single-phase, the Dittus-Boelter equation (Eq. (2.20)) is applied. The exponent of Prandtl number is 0.4 at heating and 0.3 at cooling.

Dittus-Boelter equation (1930):

$$Nu = \frac{h_{ref} d_h}{k_{ref}} = 0.023 \mathrm{Re}^{0.8} \mathrm{Pr}^{0.3 \ or \ 0.4} \tag{2.20}$$

The heat transfer coefficient becomes different at two-phase state. Chen correlation (1987) and Gungor and Winterton correlation (1987) are applied as the heat transfer coefficient for condensation and evaporation, respectively.

Chen correlation for condensation (1987):

$$\frac{h_{ref}d_h}{k_l} = 0.018\left(\frac{\mu_g}{\mu_l}\right)^{0.078}\left(\frac{\rho_l}{\rho_g}\right)^{0.39}\mathrm{Re}_l^{0.20}[\mathrm{Re}_{lo}-\mathrm{Re}_l]^{0.70}\mathrm{Pr}_l^{0.65} \quad (2.21)$$

Gungor and Winterton correlation for evaporation (1987):

$$h_{tp} = Eh_l \quad (2.22)$$

$$E = 1 + 3000\mathrm{Bo}^{0.86} + 1.12\left(\frac{q}{1-q}\right)^{0.75}\left(\frac{\rho_l}{\rho_g}\right)^{0.41} \quad (2.23)$$

$$\mathrm{Bo} = \frac{q''}{i_{fg}G} \quad (2.24)$$

During the calculation, the heat transfer coefficients were adjusted within the correlation error range to match the results of modeling and experiment data.

The calculation of pressure drop depends on the state of refrigerant. For single-phase, Eq. (2.25-27) is applied and the friction factor is different with respect to the flow type.

$$\Delta P = f\frac{L}{d}\frac{\rho v^2}{2} \quad (2.25)$$

$$f = 64/\mathrm{Re} \quad \text{Laminar flow} \quad (2.26)$$

$$\frac{1}{\sqrt{f}} = -2.0\log_{10}\left(\frac{\varepsilon/d}{3.7} + \frac{2.51}{\mathrm{Re}\sqrt{f}}\right) \quad \text{Turbulent flow} \quad (2.27)$$

The pressure drop in the two-phase state is calculated by Muller-steinhagen and Heck correlation (1986) in Eq. (2.28-30)

Muller-steinhagen and Heck correlation (1986):

$$\frac{dP}{dL} = \left(\left(\frac{dP}{dL}\right)_l + 2\left(\left(\frac{dP}{dL}\right)_g - \left(\frac{dP}{dL}\right)_l\right)q\right)G(1-q)^{1/3} + \left(\frac{dP}{dL}\right)_g q^3 \quad (2.28)$$

$$\left(\frac{dP}{dL}\right)_l = f_l \frac{G^2}{2\rho_l d} \quad (2.29)$$

$$\left(\frac{dP}{dL}\right)_g = f_g \frac{G^2}{2\rho_g d} \quad (2.30)$$

According to Shen and Groll (2005), lubricants can improve heat transfer by increasing wetted surface, but high viscosity and mass transfer resistance reduce heat transfer. The influence of the lubricant in the heat transfer process is neglected during the calculation. However, the amount of lubricant and that of refrigerant dissolved in the lubricant can not be ignored. The mass of refrigerant and lubricant in a single grid volume is calculated differently depending on the mixture state. The mass of each grid is easily obtained at subcooled state with mixture density and oil circulation ratio (OCR). OCR is the ratio between mass flow of oil and that of the mixture, assuming 1% in the modeling.

$$m_{oil} = OCR \cdot V \cdot \rho_{mix} \tag{2.31}$$

$$m_{ref} = (1 - OCR) \cdot V \cdot \rho_{mix} \tag{2.32}$$

On the other hand, mass calculation at the combined state is not simple. Two approaches are considered for the mass calculation: a 'void fraction model' and a 'film thickness model'. The 'void fraction model' calculates the mass of refrigerant and lubricant from the void fraction, which is the ratio of the tube volume (or area) occupied by the gas. This void fraction is not only a function of the vapor quality and density but also a function of other variables such as mass flux, viscosity, velocity and so on. Of the various void fraction models, the Hughmark (1964) correlation in Eq. (2.33) is used because it showed the best agreement. (Rice, 1987; LeRoy et al., 2000; Woldesemayat and Ghajar, 2007) K_H is a function of viscosity-averaged Reynolds number, Froude number and liquid volume fraction.

$$\alpha_{VF} = \frac{V_g}{V_g + V_l} = K_H / \left[1 + \left(\frac{1-q}{q}\right)\frac{\rho_g}{\rho_l}\right] \tag{2.33}$$

V is a grid volume. From this model, the mass of the oil is calculated as Eq. (2.34)

$$m_{oil,void\ \ fraction\ \ model} = \rho_l \cdot (1 - \alpha_{VF}) \cdot V \quad (2.34)$$

The other approach is the 'film thickness model' that calculates the thickness of the film formed by a liquid mixture of lubricant and refrigerant. The film thickness model is based on the assumption that the flow pattern is an annular flow. A schematic of the annular flow of the pipe and liquid film thickness is shown in Fig. 2.3. The annular flow is mainly divided into liquid film flow and gas core flow. According to Mehendale and Radermacher (2000), the following conditions are assumed in order to obtain the film thickness.

(1) Flow is fully developed, incompressible, steady-state, adiabatic and axisymmetric.
(2) The film thickness of the cross-section is uniform
(3) The fraction of liquid entrained as droplets is zero.
(4) The gas and liquid phases in a section have uniform properties.
(5) Liquid film behaves as a Newtonian fluid
(6) Axial acceleration is neglected.

The momentum equation for z-direction (Fig. 2.3) for the liquid film is Eq. (2.35).

$$\frac{u_l}{r}\frac{d}{dr}\left(r\frac{du}{dr}\right) = \frac{dP}{dz} + \rho_l g \quad (2.35)$$

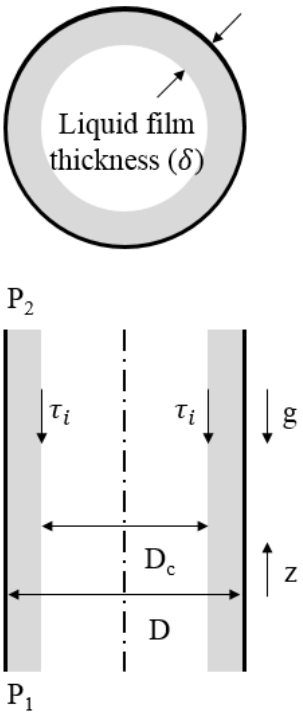

Fig. 2.3 Schematic of annular flow and liquid film thickness in pipe

By integrating this equation for r and applying the boundary condition of $\tau(r = R - \delta) = \tau_i$, Eq. (2.36) is obtained.

$$\tau = \tau_i \frac{(R-\delta)}{r} - \frac{1}{2}\left(\frac{dP}{dz} + \rho_l g\right)\left(\frac{r^2-(R-\delta)^2}{r}\right) \tag{2.36}$$

Applying the Newton's law of viscosity ($\tau = -\mu_i \frac{du}{dr}$) from the assumption (5), it gives Eq. (2.37).

$$-\mu_i \frac{du}{dr} = \tau_i \frac{(R-\delta)}{r} - \frac{1}{2}\left(\frac{dP}{dz} + \rho_l g\right)\left(\frac{r^2-(R-\delta)^2}{r}\right) \tag{2.37}$$

Integrating Eq. (2.37) with respect to r and using the no-slip boundary condition for the liquid film, $u(r = R) = 0$, Eq. (2.38) is obtained.

$$u_l = \frac{1}{\mu_l}\left(\tau_i(R-\delta) + \frac{(R-\delta)^2}{2}\left(\frac{dP}{dz} + \rho_l g\right)\right) \cdot \ln\frac{R}{r} - \frac{1}{4\mu_l}\left(\frac{dP}{dz} + \rho_l g\right)(R^2 - r^2) \tag{2.38}$$

Eq. (2.29) is the mass flow rate of the liquid film, which is calculated by integrating the velocity of the liquid film over the cross section.

$$\dot{m}_l = \frac{2\pi\rho_l}{\mu_l}\left[\tau_i(R-\delta) + \frac{(R-\delta)^2}{2}\left(\frac{dP}{dz} + \rho_l g\right)\right]\left[\frac{R^2-(R-\delta)^2}{4} - \frac{(R-\delta)^2}{2} ln\frac{R}{R-\delta}\right] - \frac{\pi\rho_l}{8\mu_l}\left(\frac{dP}{dz} + \rho_l g\right)[R^2 - (R-\delta)^2]^2 \quad (2.39)$$

In order to calculate the thickness of liquid film (δ), pressure gradient (dP/dz) and interfacial shear stress (τ_i) are required. These values are derived from momentum equation for z-direction for the gas core in Eq. (2.40) and interfacial shear stress equation in Eq. (2.41).

$$\frac{dP}{dz} + \rho_g g + \frac{\tau_i d_g \pi}{A_g} = 0 \quad (2.40)$$

$$\tau_i = \frac{1}{2} f_i \rho_g (u_g - u_l)^2 \quad (2.41)$$

The velocity of the liquid film is very small compared with that of the gas core. Wallis (1969) proposed an interfacial friction factor is in Eq. (2.42)

$$f_i = 0.005 \cdot (1 + 300 \cdot \delta/d) \quad (2.42)$$

In Eq. (2.39-42), the thickness and mass flow rate of liquid film are calculated. Then, the mass of lubricant in a single grid is obtained from Eq. (2.43-44).

$$m_{oil,film\ thickness\ model} = \rho_l \cdot (1 - w) \cdot V_l \quad (2.43)$$

$$V_l = V \cdot \left(1 - \left(1 - \frac{\delta}{R}\right)^2\right) \quad (2.44)$$

Fig. 2.4 shows the relationship between the quality of the refrigerant, the thickness of the liquid film and oil per unit length. The thickness of the liquid film is relatively thin when compared with the pipe radius except for the subcooled and low vapor quality regions because of the large difference between liquid and vapor density. On the other hand, the amount oil per unit length is high at superheated and high vapor quality regions because the fraction of lubricant in the liquid film increases at these regions.

Between the two different approaches, the 'film thickness model' is more suitable for a high quality region where annular flow can be assumed. (Radermacher et al., 2006) The 'Void fraction model' is applicable for the low quality region. Since the boundary between two models is difficult to judge, Kim and Kim (2016) suggested Eq. (2.45) that applies both methods with a weighting factor.

$$m_{oil} = m_{oil,film\ thickness\ model} \cdot q + m_{oil,void\ fraction\ model} \cdot (1 - q) \quad (2.45)$$

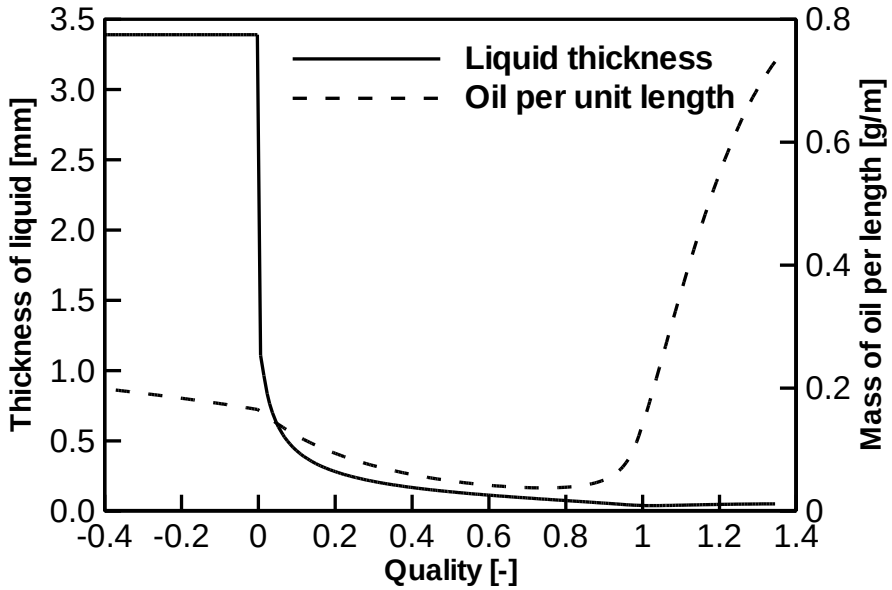

Fig. 2.4 Quality vs. thickness of liquid and oil per unit length (residential system)

From the above equations, the mass of refrigerant and lubricant is determined in a single grid volume. After calculating a single grid volume, the calculation of entire heat exchanger is required. The flow path is one of the essential factors to consider in the heat exchanger modeling. Fin-tube heat exchangers usually distribute the main flow to multiple flows, and each path undergoes a different heat exchange process. In this study, target systems have condensers with a counter-cross flow, which means the flow between air and refrigerant is basically cross-flow, but the air inlet is on the opposite side of the refrigerant inlet. The inlet condition of air and refrigerant is known. However, in a counter-cross flow, one of the exit condition for air or refrigerant need to be assumed in order to calculate the condenser. On the contrary, the evaporators have a parallel-cross flow. Schematics of flow paths in the target systems at cooling condition is shown in Fig. 2.5. Three-dimensional heat exchanger modeling was done. The mass flow rate of each path is assumed to be the same.

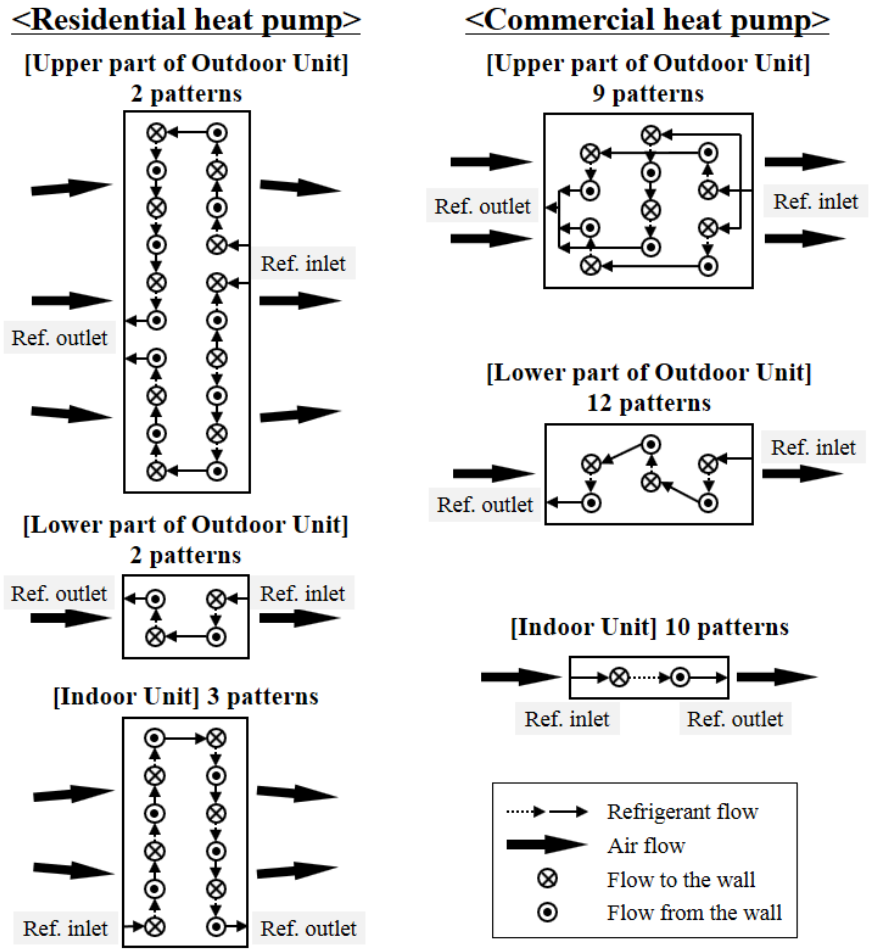

Fig. 2.5 Flow paths in target residential and commercial heat pump at cooling mode

2.4 Cycle modeling

Steady-state modeling was done to provide a reasonable description of the target heat pump systems. Fig. 2.6 represents the overall calculation flow chart for the system. Cycle modeling is largely divided into two parts. During the operation, suction DSH is usually kept constant at the target value to prevent wet compression. For this reason, setting the target DSH during cycle modeling is a reasonable assumption under normal operating conditions. However, according to Yoo et al. (2017), when a refrigerant leak occurs, the EEV opening increases. (Further explanation will be given in Chapter 3) Theoretically, the area of EEV cannot exceed its maximum possible value. When the EEV opening reaches its maximum, DSH is no longer controllable and a different approach is required in the modeling. The left side of the flow chart in Fig. 2.6 is applied when the suction DSH is in the controllable region. Initial conditions, such as geometry, outdoor and indoor air temperature and humidity conditions, OCR, need to be given. Specific geometry values are listed in Table 2.1 for residential heat pump and Table 2.2 for commercial heat pump. The air mass flow rate is also determined initially. Operating conditions are given in Table 2.3, and 2.4. The target values such as mass charge of refrigerant and lubricant in the system and suction DSH are decided. The pressure at the inlet and outlet of the compressor is mainly adjusted during the calculation. First, the

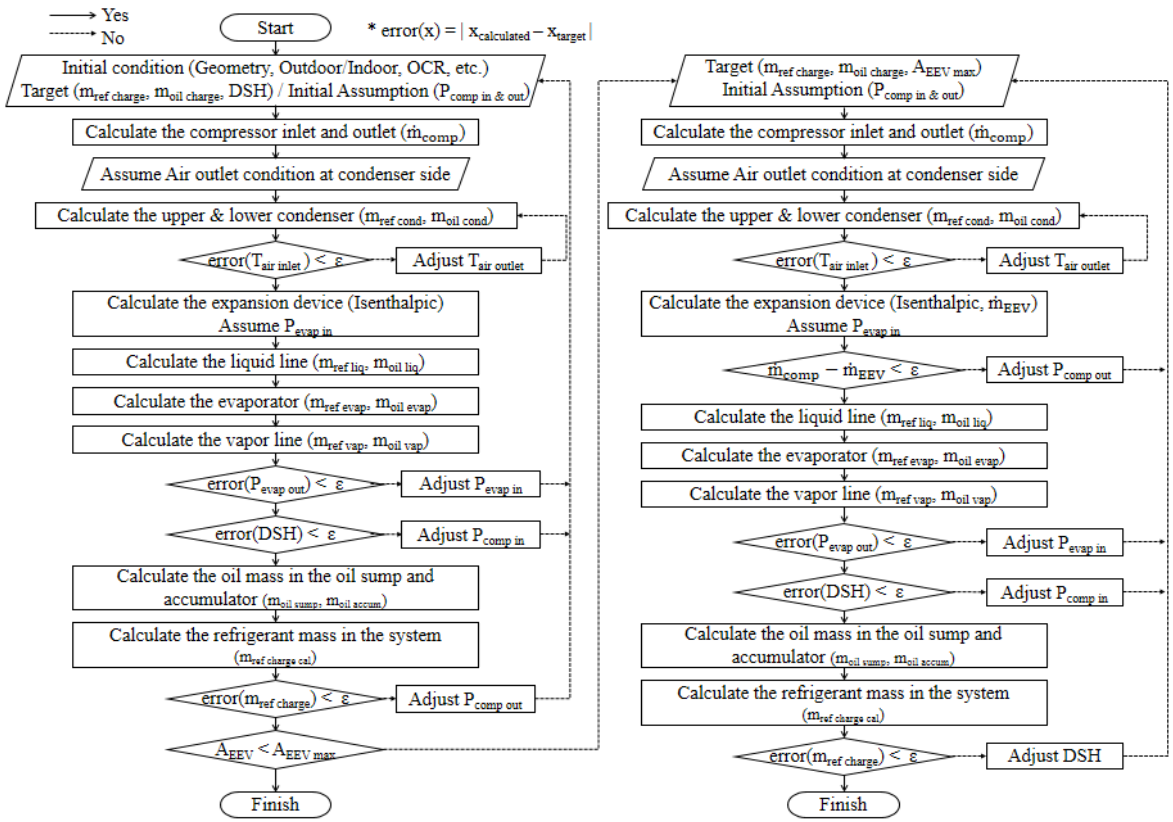

Fig. 2.6 Calculation flow chart of heat pump cycle modeling

Table 2.1 Specification of each component (Residential heat pump)

Part	Specifications	Value
Compressor	Displacement volume (cm^3)	10.2
	Sump diameter / height (mm)	103 / 50
Accumulator	Diameter / height (mm)	75 / 220
Condenser	Width / length / height (mm)	850 / 36 / 504
	Tube inner / outer diameter (mm)	6.78 / 7.34
	Tube transverse / longitudinal pitch (mm)	21 / 18
	Fin pitch (mm)	1.5
	Flow path row / step	2 / 24
Evaporator	Width / length / height (mm)	583 / 20 / 360
	Tube inner / outer diameter (mm)	5.9 / 4.5
	Tube transverse / longitudinal pitch (mm)	20 / 10
	Fin pitch (mm)	1.5
	Flow distribution row / step	3 / 12
EEV	Maximum area : $A_{EEV,max}$ (mm^2)	1.99

Table 2.2 Specification of each component (Commercial heat pump)

Part	**Specifications**	**Value**
Compressor	Displacement volume (cm^3)	62.1
	Sump diameter / height (mm)	200 / 20
Accumulator	Diameter / height (mm)	150 / 1100
Oil separator	Diameter / height (mm)	100 / 250
Condenser	Width / length / height (mm)	1650 / 60 / 1220
	Tube inner / outer diameter (mm)	6.78 / 7.34
	Tube transverse / longitudinal pitch (mm)	20 / 21
	Fin pitch (mm)	1.7
	Flow path row / step	3 / 58
Evaporator	Width / length / height (mm)	3000 / 40 / 200
	Tube inner / outer diameter (mm)	6.78 / 7.34
	Tube transverse / longitudinal pitch (mm)	20 / 20
	Fin pitch (mm)	1.7
	Flow distribution row / step	2 / 10
EEV	Maximum area : $A_{EEV,max}$ (mm^2)	10

Table 2.3 Calculation and experiment conditions for cooling mode (Residential heat pump)

Variables	**Value**		
Refrigerant	R410A		
Refrigerant charge amount (g)	400 - 1200 (Δ=100)		
Lubricant	Polyvinyl ether(PVE) type		
Lubricant charge amount (g)	300		
DSH (K)	5 (or maximum EEV opening)		
Air condition (ISO 5151)	Rating	Maximum	Minimum
Indoor air inlet dry bulb temperature (˚C)	27.0	32.0	21.0
Indoor air inlet wet bulb temperature (˚C)	19.5	23.0	15.0
Outdoor air inlet dry bulb temperature (˚C)	35.0	43.0	21.0
Outdoor air inlet wet bulb temperature (˚C)	24.0	26.0	15.0
Compressor speed (Hz)	50	40	48

Table 2.4 Calculation and experiment conditions for cooling mode (Commercial heat pump)

Variables	**Value**			
Refrigerant	R410A			
Refrigerant charge amount (kg)	6 - 11 (Δ=1)			
Lubricant	Polyvinyl ether(PVE) type			
Lubricant charge amount (kg)	3			
DSH (K)	5, 10, 15 (or maximum EEV opening)			
Air condition (ANSI/AHRI 1230)	Rating	Maximum	Minimum	Condensate
ID inlet DB (˚C)	26.7	26.7	19.4	26.7
ID inlet WB (˚C)	19.4	19.4	13.9	23.9
OD inlet DB (˚C)	35.0	46.1	19.4	26.7
OD inlet WB (˚C)	23.9	23.9	13.9	23.9
Compressor speed (Hz)	60, 100	60, 100	60	60, 100

compressor is calculated according to Section 2.3.1. After that, the upper and lower part of condenser are calculated with the assumption of either the outlet of air or that of refrigerant. Expansion valve, liquid lines, evaporators and vapor lines are calculated consecutively. The outlet state of the vapor line is treated the same as accumulator and compressor inlet because the distance between these components is very close. The calculated state of vapor line outlet is compared with the assumed state of the compressor inlet. Pressure at evaporator inlet and compressor inlet are continuously adjusted until these two states match. After cycle match process, the refrigerant charge amount between calculated and target value is compared. The oil charge amount in the compressor oil sump and accumulator is obtained from the initial oil charge and the amount of oil at the other parts. Assuming that the compressor oil sump has a constant liquid level, the final refrigerant charge amount is acquired. If this value is different from the target charge amount, the pressure at the compressor outlet is adjusted. If the calculated values (DSH, refrigerant ant oil charge amount) satisfy the target values, the area of EEV is calculated according to Section 2.3.3. This is because the mass flow rate from the compressor is equal to that from EEV. If the EEV area exceeds the maximum possible value, the calculation starts on the right side of the Fig. 2.6. One of the target values is changed from suction DSH to EEV opening. This is because EEV opening

value is fixed at the maximum value at low charge region. The calculation procedure is similar except for the different adjustment variables. This calculation requires one more iterative process. The mass flow rate at the compressor and EEV need to be the same, so the pressure at the compressor outlet is adjusted to match these values. The pressure of the evaporator and compressor inlet is controlled to match the outlet state of vapor line and the inlet of the compressor. Finally, suction DSH is adjusted in order to coincide the calculated charge amount with assumption. Throughout this process, the performance at each charge amount can is derived.

2.5 Modeling results and discussion

Previously from Figs. 2.1 and 2.2, the difference in optimal charge amount between experiment and modeling was 22% and 11% for the residential and commercial system when the lubricant is not considered in the modeling at rating cooling condition. Figs. 2.7 and 2.8 show the same data but the results from modeling with lubricant are added. In residential system, the optimal charge amount in the modeling with lubricant is 900 g, which is the same value from the experiment. In commercial system, the optimal charge amount in the modeling with lubricant is 9 kg, which also matches with experiment data. The same trends are also shown at different temperature conditions. Table 2.5 represents the optimal charge amount at various temperature conditions from the experiment and modeling. At maximum cooling condition in residential system, the optimal charge amount from the experiment is 1000 g but from modeling without lubricant, it was only 800 g. However, after lubricant is considered, the optimal charge amount increased to 1000 g, which coincides with experiment data. Similarly, the optimal charge amount at other conditions increased compare with experimental results. From these results, it can be seen that considering the lubricant in the heat pump modeling has a great influence on the calculation of the refrigerant charge amount by about 10 to 30%

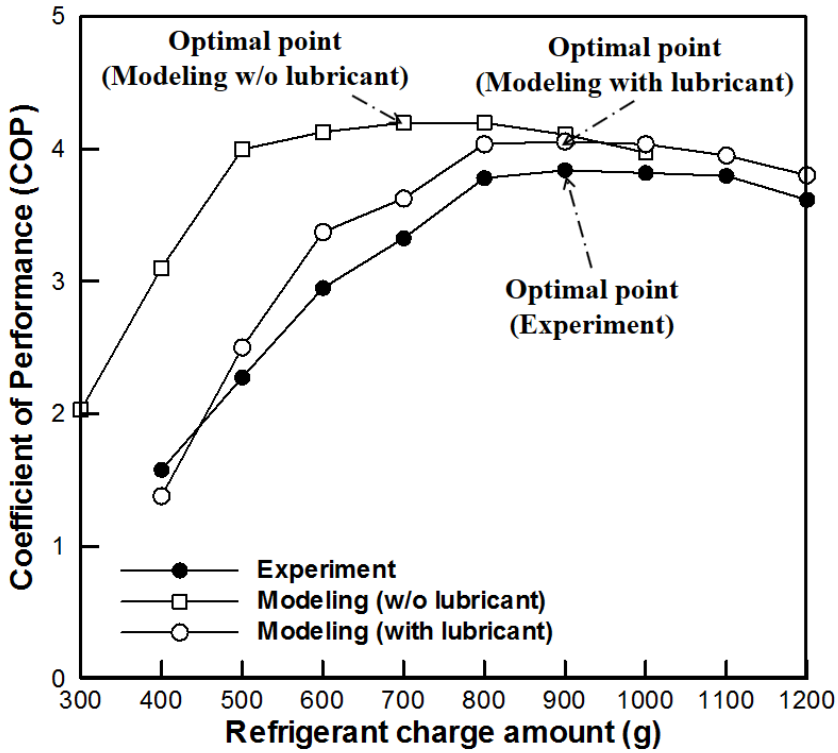

Fig. 2.7 Refrigerant charge amount versus coefficient of performance in experiment, modeling with and without lubricant at rating condition (residential heat pump)

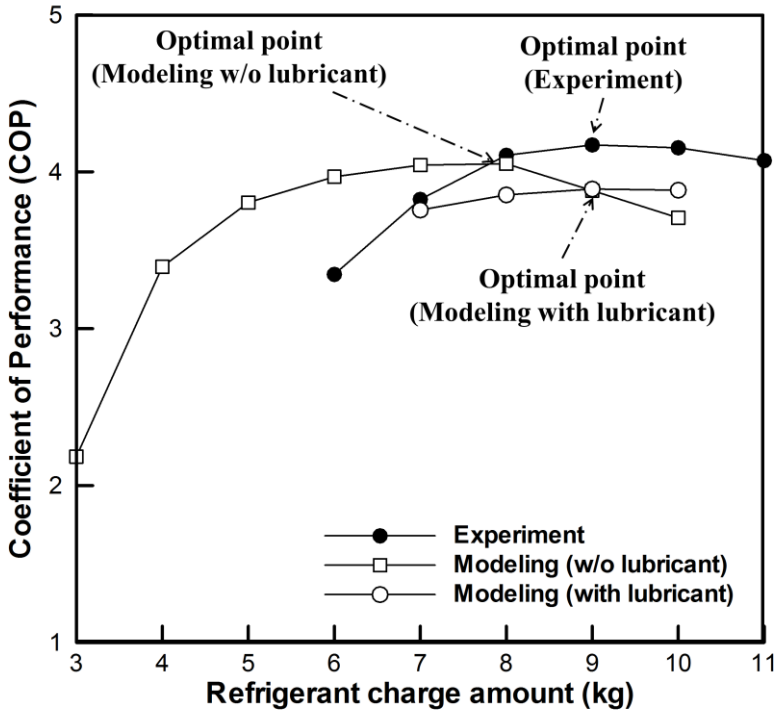

Fig. 2.8 Refrigerant charge amount versus coefficient of performance in experiment, modeling with and without lubricant at rating condition (commercial heat pump)

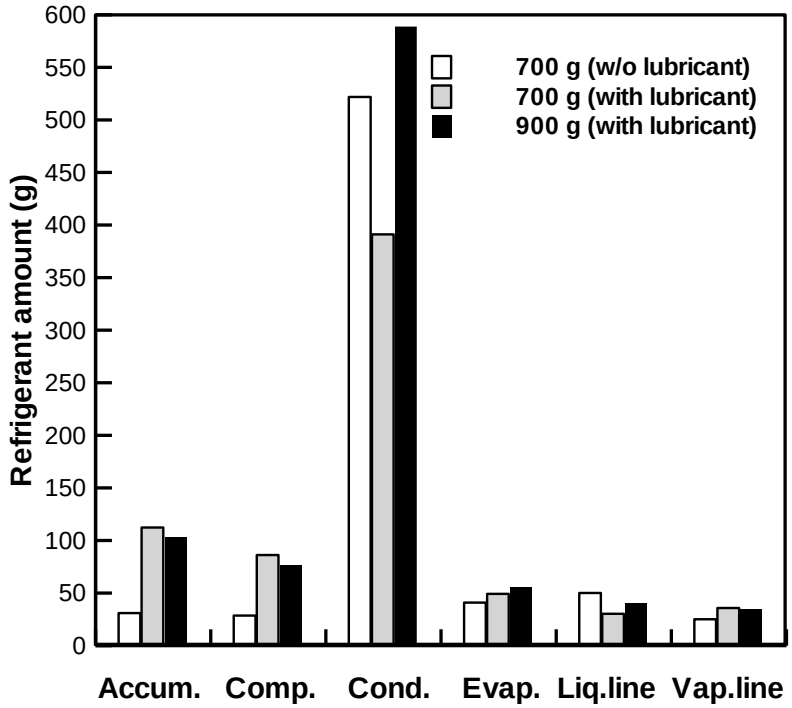

Fig. 2.9 Refrigerant charge amount at each component from the modeling with and without lubricant at rating condition (residential heat pump)

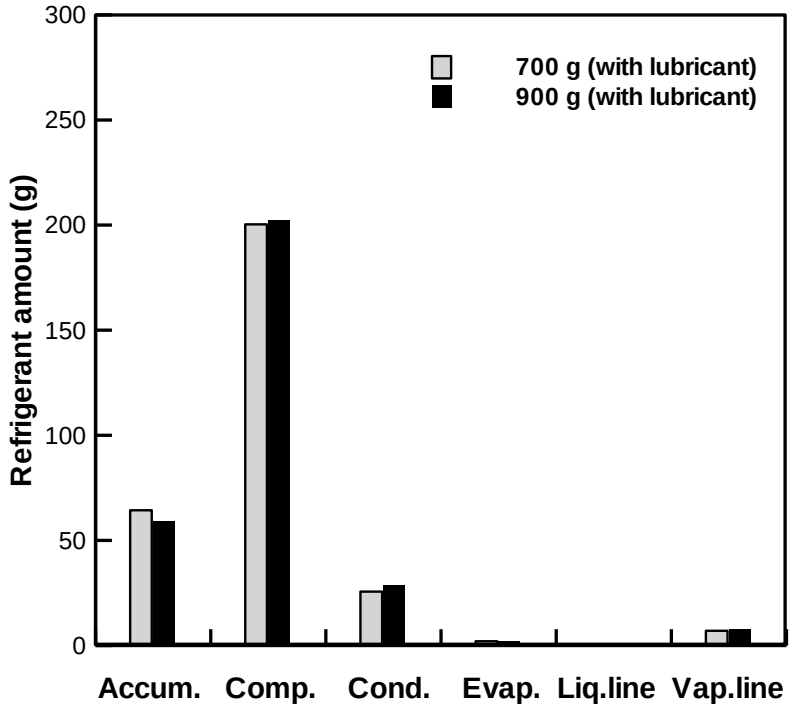

Fig. 2.10 Lubricant charge amount at each component from the modeling with lubricant at rating condition (residential heat pump)

Table 2.5 Optimal charge amount from experiment and modeling with and without lubricant (Residential and commercial heat pump)

Air condition (ISO 5151 – Residential heat pump)	**Rating**	**Maximum**	**Minimum**
Optimal charge amount (g) (Experiment)	900	1000	1000
Optimal charge amount (g) (Modeling without lubricant)	700	800	600
Optimal charge amount (g) (Modeling with lubricant)	900	1000	900

Air condition (ANSI/AHRI 1230 – Commercial heat pump)	**Rating**	**Maximum**	**Minimum**	**Condensate**
Optimal charge amount (kg) (Experiment)	9	9	8	9
Optimal charge amount (kg) (Modeling without lubricant)	8	8	7	8
Optimal charge amount (kg) (Modeling with lubricant)	9	9	8	9

Fig. 2.9 and 2.10 represent the refrigerant and lubricant charge amount, respectively, at each component from the modeling with and without lubricant at rating condition in the residential heat pump. Three different conditions are chosen in this bar graph. The white bar represents the condition of the charge amount of 700 g without lubricant in the calculation because it is optimal charge amount point. The gray bar is at the charge amount of 700 g with lubricant in consideration and the black bar is at the optimal charge amount condition (900 g) when lubricant is concerned. When comparing the white and gray bars in Fig. 2.9, the refrigerant charge amount at condenser is significantly different. This is because the amount of refrigerant in accumulator and compressor is much larger when lubricant is considered. In Fig. 2.10, the amount of lubricant is the highest in the compressor and is larger in the order of the accumulator and the condenser. Thereby, the refrigerant amounts of these components are important. In compressor and accumulator, it increases from 28 to 86 g and from 31 to 112 g. respectively. The total difference is 138 g, which is a significant amount. Conversely, the amount of refrigerant decrease from 522 to 391 g, which makes the total charge amount at the same for both conditions. When the white and black bars are compared, which are the optimal charge amount condition without and with lubricant respectively, refrigerant charge amount increases at the most of the component when lubricant is in the calculation. The refrigerant

amount in compressor, accumulator and condenser are increases 72, 48 and 67 g respectively and the total amount is 187 g which compensates the difference between the optimal point from the modeling without and with lubricant. This shows that the amount of refrigerant dissolved in the lubricant is not negligible. Between the two possible factors that were mentioned in Section 2.1, uneven flow distribution only contributes around 5 %. (Peuker, 2010). On the other hand, the lubricant effect is much more significant.

2.6 Summary

The optimal refrigerant charge amount obtained from the modeling is generally underestimated compare with experimental data when the lubricant is not considered. In this chapter, the heat pump modeling with and without lubricant is conducted. The property equations of refrigerant and lubricant mixture, such as solubility, viscosity and enthalpy are acquired. With these equations, the modeling of the accumulator, compressor, heat exchangers, electronic expansion valve, liquid line and vapor line is done. After the component modeling, cycle modeling is carried out to match the refrigerant and lubricant charge amount and suction DSH. If the EEV area exceeds its theoretical maximum possible value, the modeling process becomes different from the assumption of suction DSH to EEV area.

The calculation of lubricant significantly affect the modeling results. The optimal charge amount difference that comes from the lubricant consideration is around 10 to 30%. Comparing with the flow path and distribution factor, which is around 5%, lubricant clearly is the most important factor in the heat pump modeling especially when charge amount is concerned.

Chapter 3. The detection method of refrigerant leakage amount from limited sensor installation in residential heat pump systems

3.1 Introduction

This chapter describes how to detect the amount of refrigerant leakage in a residential air heat pump system. From the previous research papers in the section 1.2.2, the majority suggests DSH and DSC as a significant indicator for leakage amount detection. In order to get DSH at least two sensors are required. One is the pressure or a temperature sensor to measure the evaporating temperature and the other is the temperature sensor at the compressor inlet side. The number of sensors required to obtain DSC is also two. However, residential air heat pumps generally do not allow many sensors because of cost. The useful and measurable information from the heat pump is temperature, pressure and mass flow rate, etc. Among them, the temperature measurement cost is the lowest. For this reason, pressure transducers and mass flow meters are not installed. The number of temperature sensors in this study is limited to five. The measurement points are air inlet of the indoor and outdoor side, evaporator and

condenser midpoints and compressor discharge point. Additionally, the EEV opening, the rotational speed of the compressor and the fan are useful information.

The goal of this study is to suggest the simplest and a reasonable method to detect leakage amount in residential heat pump systems. If the amount of refrigerant in the system is less than half of the optimal charge amount, the system pressure drops noticeably, as shown in Fig.1.5. Therefore, it is easy to find out the leakage amount in this range. However, when the charge amount is reduced by about 30% from optimal charge amount, the capacity of the system decreases to 20 ~ 30%. For this reason, the method should detect refrigerant leakage before its amount exceeds 30% of the optimal charge amount.

The proposed method in this study is based on the temperature difference between the indoor air inlet and the evaporator midpoint. This is clearly simple and detail explanation is given in this chapter. The term ‘leakage amount’ is defined as the refrigerant amount that has been the leak from the optimal charge amount of the system. Thereby, the leaked condition can be treated as undercharge condition. For this reason, the term ‘charge’ is used more often instead of ‘leakage’ in this chapter and chapter 4.

3.2 Experimental setup

3.2.1 Residential heat pump setup and experimental condition

For the experiment, one of the residential heat pump, which has a nominal capacity of 4 kW, was chosen. Fig. 3.1 shows the picture of the indoor and outdoor unit of the heat pump. This heat pump has a variable-speed rotary type compressor and an electronic expansion valve (EEV). Fig. 3.2 represents the schematic of the experiment setup. The outdoor unit consists of accumulator, compressor, condenser and EEV. The indoor unit only has evaporator. Each unit is installed in the outdoor and the indoor side of the conditioned chamber, respectively. The main role of this conditioned chamber is to set the environment at the target air condition.

For air side, the dry and wet bulb temperature of indoor and outdoor chambers are measured with resistance temperature detectors (RTD). With the air conditioners and heaters, which have a capacity of 30 kW, the chambers can set the temperature from -30 to 60˚C for the outdoor condition and 5 to 50˚C for the indoor condition. The relative humidity for both chambers can be adjusted from 20 to 90%. With the temperature data, air density and enthalpy is also derived from ASHRAE Handbook (2009). Inside the indoor chamber, wind

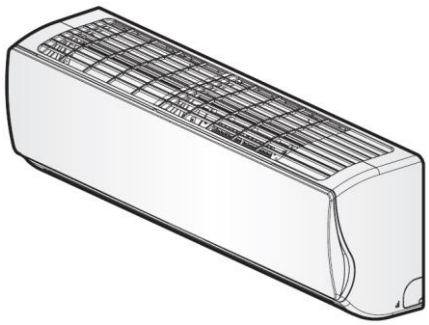

(a) Indoor unit

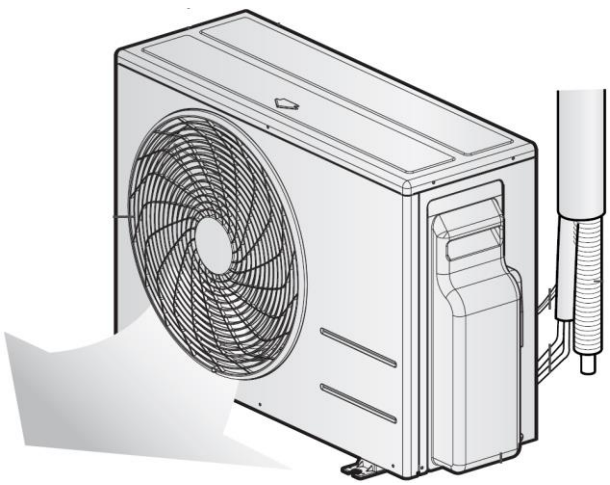

(b) Outdoor unit

Fig. 3.1 Residential air heat pump (target model)

tunnel and nozzle exists and the pressure difference between nozzle inlet and outlet is measured to obtain the mass flow rate of air from the indoor unit fan. The air mass flow rate is calculated according to ANSI/AMCA 210 (2007). The measurement points of the air side are shown as white square in Fig. 3.2.

For the refrigerant side, mass flow rate, pressure and temperature are measured to get information from the system. When the system reaches a steady-state condition, the mass flow rate is the same throughout the system. For this reason, one Coriolis type mass flow meter is used. The pressure transducer is applied at the inlet and outlet of condenser and evaporator. The thermocouple is attached to the point of inlet and outlet of each component. The measurement points of the refrigerant side are presented as gray circles in Fig. 3.2. However, residential heat pumps have limited sensor information and the target system only measures the temperature at five points, which are the air inlet of indoor and outdoor side, condenser and evaporator midpoint and compressor discharge. These five points are also shown as black circles in Fig. 3.2. Additionally, power consumption is measured with a power meter. The specification of measurement instruments is summarized in Table 3.1.

In order to find out the optimal charge amount of the target system, experiments with various refrigerant charge amount are required. Optimal charge amount is determined at the point where COP becomes maximum. The

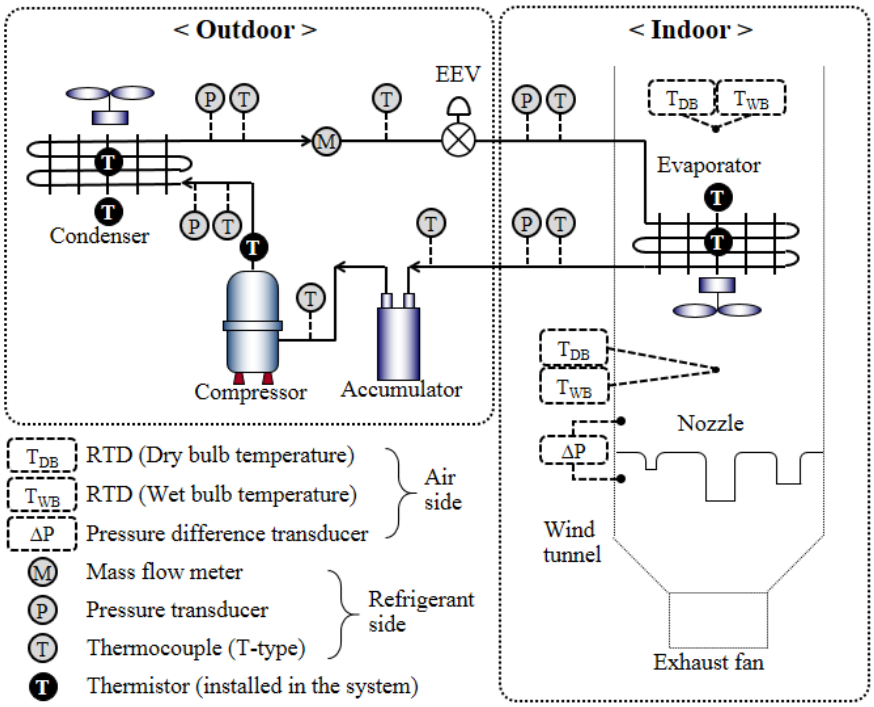

Fig. 3.2 Schematic of experiment setup (residential heat pump)

Table 3.1 Specifications of measurement instruments

Mass flow meter (Refrigerant side)	
Model	Oval, CA015G21SA22AA1132
Type	Coriolis
Range	0~100 g/s
Accuracy	±0.5% F.S.
Thermocouple T-type (Refrigerant side)	
Model	Omega TT-T-30-SLE
Range	-267 ~ 260˚C
Accuracy	±0.7˚C
Thermistor (installed in the system - Refrigerant side)	
Model	MITSUBISHI Materials, ACD-45
Range	-30 ~ 130˚C
Accuracy	±0.5˚C
Resistance Temperature Detector (Air side)	
Model	Netsushin, NR-351(PT 100Ω)
Range	-200 ~ 250˚C
Accuracy	(0.15+0.002|T|) ˚C

Table 3.1 Specifications of measurement instruments (continued)

Absolute pressure transducer (Refrigerant side)	
Model	KELLER PA-21Y
Range	0~5000 kPa, 0~6000 kPa
Accuracy	±0.25% F.S.
Differential pressure transducer (Air side)	
Model	Yokogawa, EJA-110A
Range	0~100 mmAq
Accuracy	±0.2% F.S.
Power meter	
Model	Yokogawa, WT 230
Range	0~1500 W
Accuracy	±0.1% of reading + 0.1% of range

Table 3.1 Specifications of measurement instruments (continued)

Multi-channel recorder	
Model	Yokogawa, DA 100 Expendable type
Number of channels	160 channels
A/D integration time	±0.25% F.S.
Compensation accuracy for reference junction	0.5C or 0.4%
Maximum resolution	1 mV, 0.1C
Measurement accuracy	±（0.05% of reading + 0.7C) ±（0.05% of reading + 2 digits)

specification of each component and experimental condition for residential heat pump system is the same as that in Table 2.1 and 2.3, respectively. During the experiment, DSH is kept 5 K but when refrigerant charge amount becomes significantly low compared with optimal charge, keeping DSH is longer available. At this condition, EEV is kept fully open. Three different air side conditions are chosen for residential heat pump according to ISO 5151 (2010) The rotational speeds of compressor among the temperature conditions are not the same because of the discharge temperature limit.

The data from the experiment are monitored by Labview program and are recorded every two seconds when the system reached a steady-state condition. (Kim et al. 2008)

3.2.2 Data reduction and uncertainty analysis

In order to obtain the capacity and COP, Eqs. 3.1 and 3.2 are needed.

$$Q_{air} = \rho_{air}\dot{V}_{air}(i_{air,in} - i_{air,out}) \quad (3.1)$$

$$COP = Q_{air}/W \quad (3.2)$$

The uncertainty of the measurement and the derived data of the experiment is presented in Table 3.2. From the data, the mass flow rate of air, cooling

Table 3.2 Uncertainty analysis at rating condition

Measurements	**Fixed error**	**Random error**	**Total error**
Pressure transducer (condenser side)	0.60%	0.39%	0.71%
Pressure transducer (evaporator side)	1.34%	0.27%	1.37%
Dry bulb air inlet temperature (RTD)	0.20 K	0.02 K	0.20 K
Wet bulb air inlet temperature (RTD)	0.19 K	0.06 K	0.20 K
Dry bulb air outlet temperature (RTD)	0.18 K	0.01 K	0.18 K
Wet bulb air outlet temperature (RTD)	0.18 K	0.03 K	0.18 K
Thermocouple (T-type)	0.50 K	1.52 K	1.60 K
Thermistor	0.70 K	0.32 K	0.76 K
Mass flow rate (refrigerant)	3.07%	0.77%	3.16%
Mass flow rate (air)	4.61%	0.50%	4.64%
Power consumption	0.20%	0.65%	0.68%
Cooling capacity	6.28%	1.19%	6.39%
COP	6.28%	1.55%	6.47%

capacity and COP are derived values from other measurements. In this case, the propagation of error method in Eq. 3.3 is applied.

$$\delta u = \left[\sum_{i=1}^{N} \left(\frac{du}{du_i}\delta u_i\right)^2\right]^{1/2} \quad (3.3)$$

Maximum error for cooling capacity and COP are 6.39% and 6.47% respectively on 95% confidence level. According to ASHRAE Guideline 2 (2010), the fractional uncertainty in the COP should not be greater than 10% and it is satisfied in this experiment.

3.3 Results and discussion

3.3.1 Effect of refrigerant charge on cycle performance

Before dive into the detection method, the performance variation with respect to charge amount is required. Fig. 3.3 shows COP at different charge amount. The maximum COP is shown at 900 g for rating condition and 1000 g for maximum and minimum condition thereby optimal charge amount of this system was chosen to 1000 g. With this optimal charge amount, 'refrigerant charge level' is defined in Eq. 3.4.

$$Refrigerant\ \ charge\ \ level\ \ (\%) = \frac{current\ \ charge\ \ amount}{optimal\ \ charge\ \ amount} \times 100 \tag{3.4}$$

By defining the charge level, the results of this study can be applied to other systems with different optimal charge amount. At the charge level of 50%, which is the half of the optimal charge, COP significantly decreases around 40 to 60% from the maximum value depending on the temperature condition. The detection of leakage at this level is essential. To explain overall performance change with respect to charge level, the pressure-enthalpy diagram in Fig. 3.4

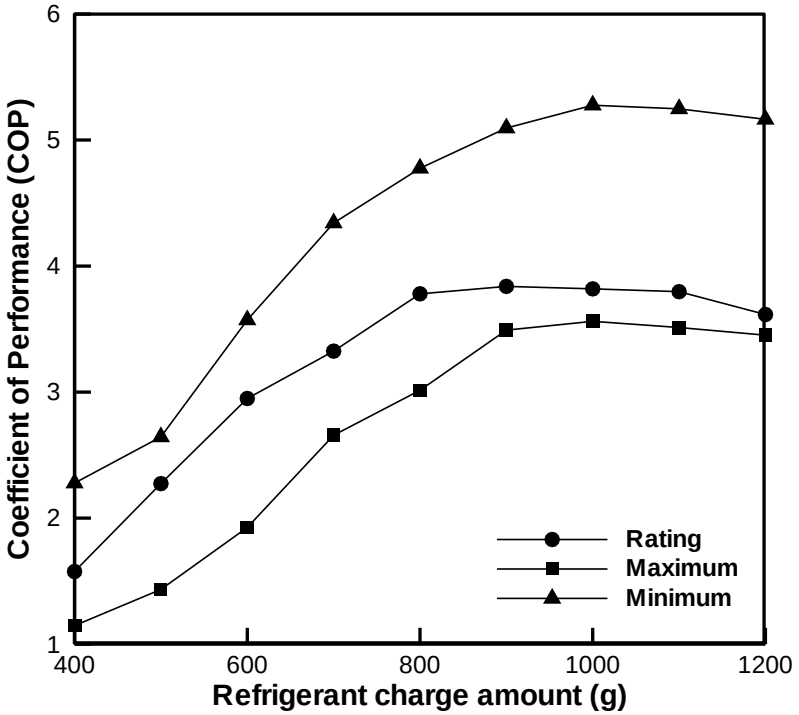

Fig. 3.3 Charge amount versus coefficient of performance (COP)

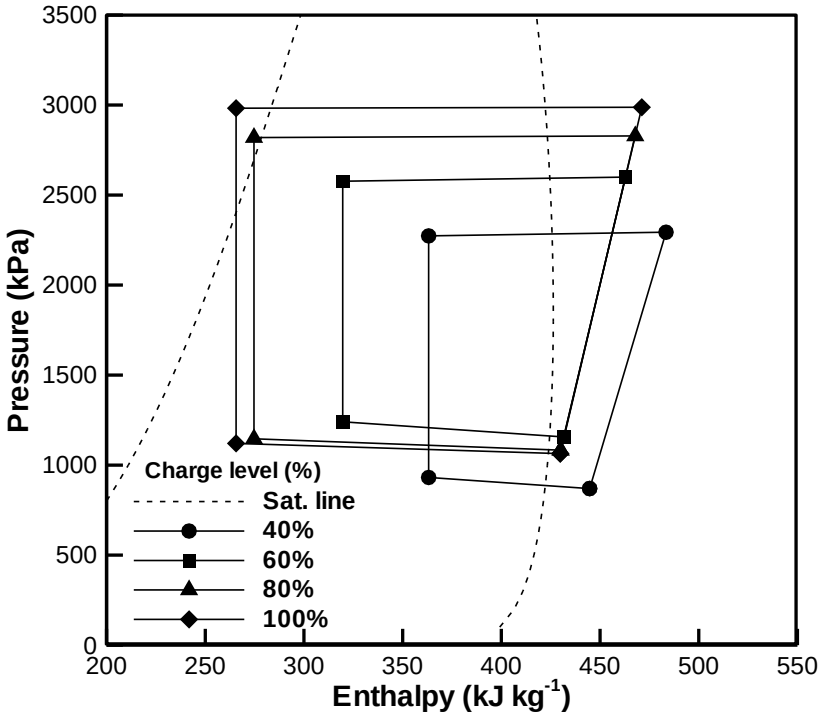

Fig. 3.4 Pressure-enthalpy diagram at rating condition

is shown. At optimal charge amount, which is a charge level of 100%, refrigerant at condenser outlet is in a subcooled state. Condensing pressure at this point is highest while evaporating pressure is not. At the charge level of 80%, refrigerant state at condenser outlet becomes a saturated liquid state. Until this point, DSH is kept at 5K. At low charge region (40 and 60%), DSH becomes larger than the target value because EEV opening reaches its maximum. The state of the condenser outlet is two-phase because there is not enough refrigerant to hold condensing pressure high so it is much lower compared with normal condition. As a result, the condensing temperature is low and the heat exchange amount between air and refrigerant at condenser is reduced. Fig. 3.5 represents DSH and EEV opening at rating condition. EEV regulates valve opening to controlled the DSH of the system. When the system has charge level over 60%, keeping DSH is available because EEV opening is between fully closed (0%) and full opened (100%) state. The sharp change of EEV opening at charge level between 60 and 90% is due to the EEV control process to hold DSH at 5K. When charge level becomes lower than 60%, the area of EEV reaches its maximum limit and DSH starts to rise. The DSH rapidly increases as charge level becomes lower from this point. Fig. 3.6 displays the condensing and evaporating pressure for different charge levels at rating condition. The condensing pressure becomes lower as leakage amount becomes

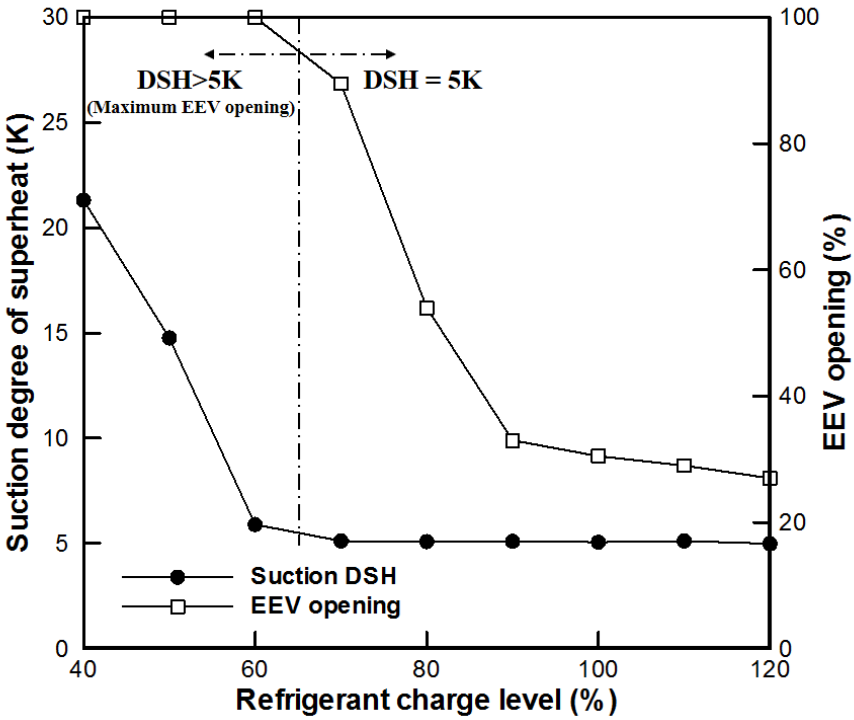

Fig. 3.5 Charge level versus suction degree of superheat and EEV opening at rating condition

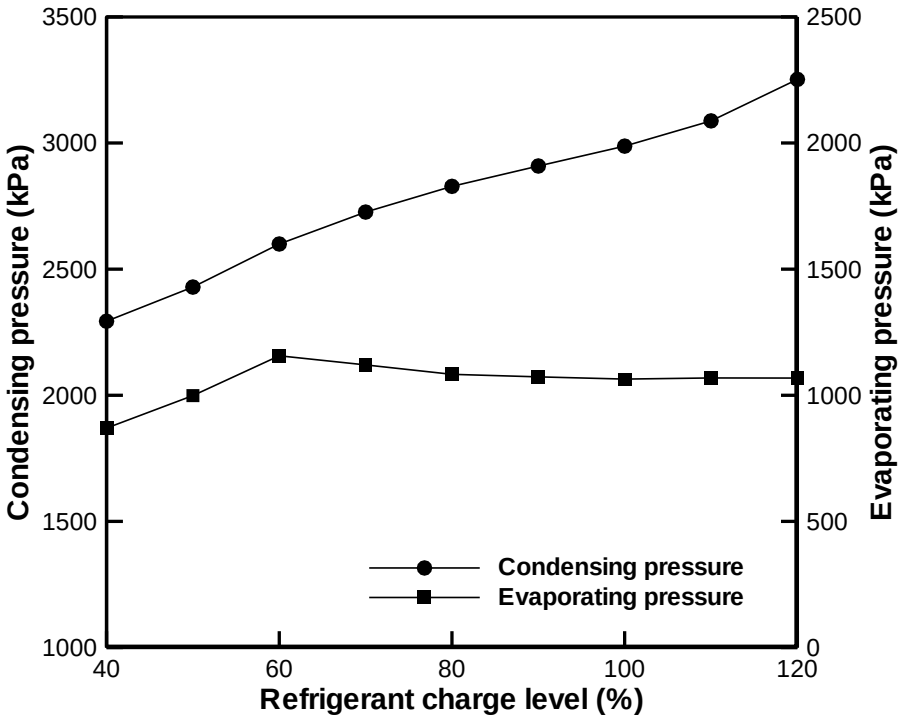

Fig. 3.6 Charge level versus condensing and evaporating pressure at rating condition

higher because there is not enough refrigerant to keep the pressure at the proper level. The evaporating pressure shows a different trend. In the region where DSH is controllable, it increases as charge level drops because of the opening of EEV increases. Conversely, evaporating pressure decreases at low charge level because EEV is fixed to maximum opening condition and lower amount of refrigerant makes system pressure level decreases. Fig. 3.7 shows cooling capacity at three different temperature condition. When the charge level decreases, system capacity goes down. The trend is similar compared with most of the previous studies. (Kim et al., 2007; Corbera´n et al., 2008; Corbera´n et al., 2011; Kim et al., 2014) This is because heat transfer rate in condenser decreases as condensing temperature becomes closer to the outdoor air temperature. Consequently, the enthalpy difference between inlet and outlet of evaporator reduces which lowers cooling capacity. Fig. 3.8 shows quality or DSC at condenser outlet. The condenser outlet is normally designed to be at subcooled state but when charge level is low, it becomes the two-phase state. DSC is calculated from condensing temperature and the temperature at condenser outlet. In order to calculate quality, enthalpy at condenser outlet needs to be obtained from Eqs. 3.5 and 3.6.

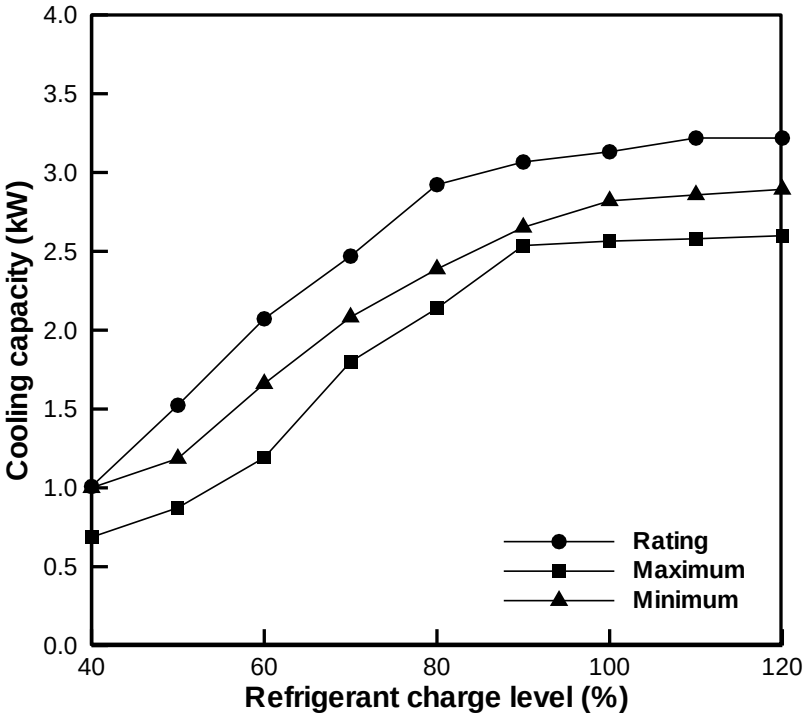

Fig. 3.7 Charge level versus cooling capacity

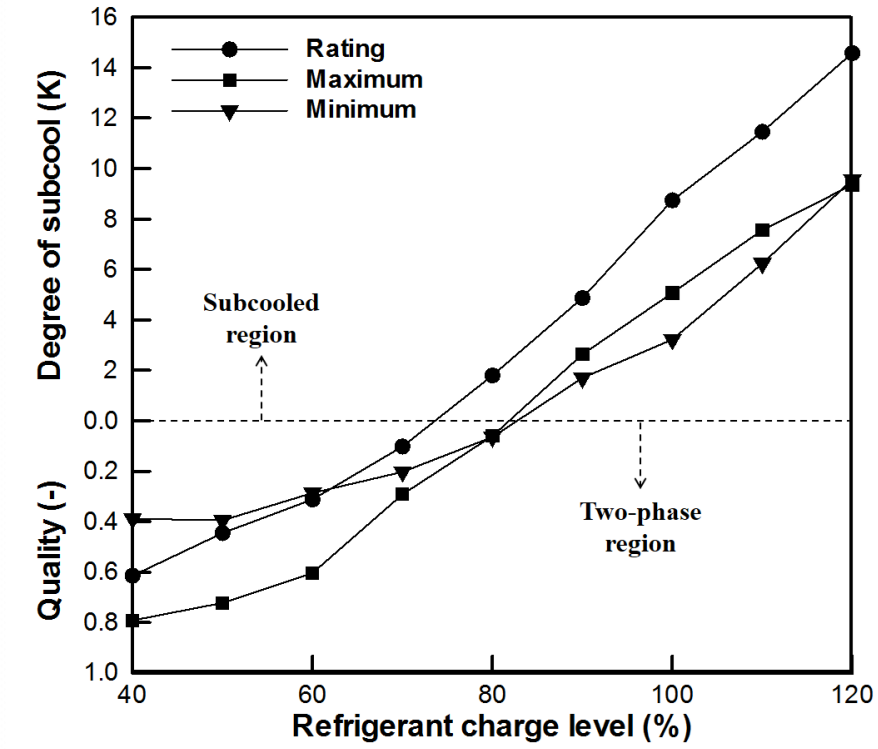

Fig. 3.8 Charge level versus quality or degree of subcool at condenser outlet

$$Q = \dot{m}_{air}(i_{air,in} - i_{air,out}) = \dot{m}_{ref}(i_{ref,evap\ out} - i_{ref,evap\ in}) \quad (3.5)$$

$$i_{ref,evap\ in} = i_{ref,cond\ out} \quad (3.6)$$

Enthalpy of evaporator inlet can be derived from Eq. 3.5, as the cooling capacity of air and refrigerant side are the same, and the enthalpy is considered to be the same as the enthalpy of condenser outlet. This is because of the isenthalpic process in EEV that is written in Eq. 3.6. At the rating temperature condition in Fig. 3.8, at the charge level higher than 80% leads the refrigerant to a subcooled state and as charge level gets higher, DSC also gets larger. However, when the charge level is lower than 80%, condensing pressure drops, which lowers the average temperature difference between air and refrigerant. Thereby, the amount of heat transfer from the refrigerant to air is decreased and refrigerant does not fully condense at condenser outlet. In addition, the vapor quality of the refrigerant at the condenser outlet rises, as charge level becomes smaller.

Fig. 3.9 shows the mass flow rate of the refrigerant in the system. The mass flow rate is proportional to the density at the compressor inlet and the density of the refrigerant is a strong function of evaporating pressure and DSH. At the rating condition in Figs. 3.6 and 3.7, at the range of charge level below 60%,

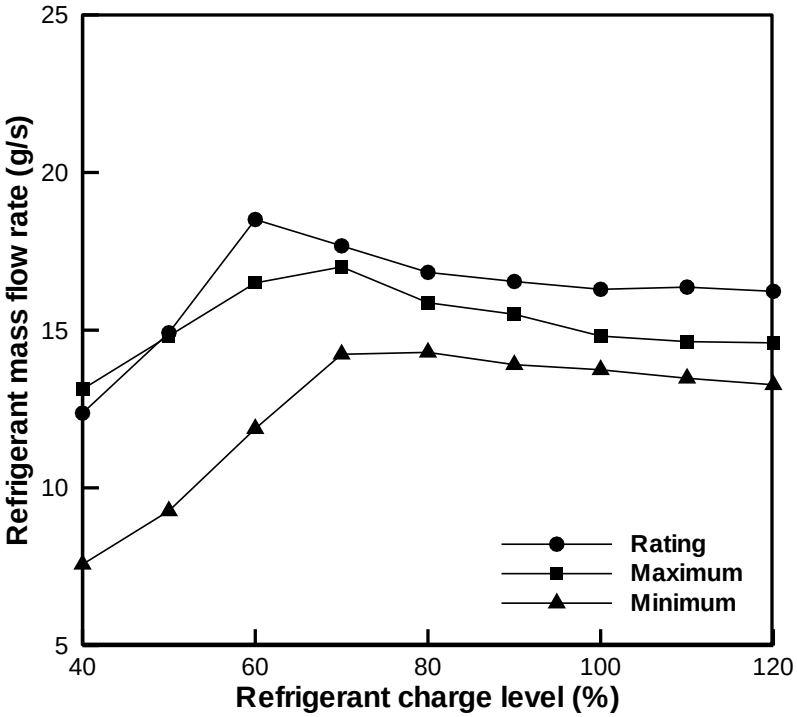

Fig. 3.9 Charge level versus refrigerant mass flow rate

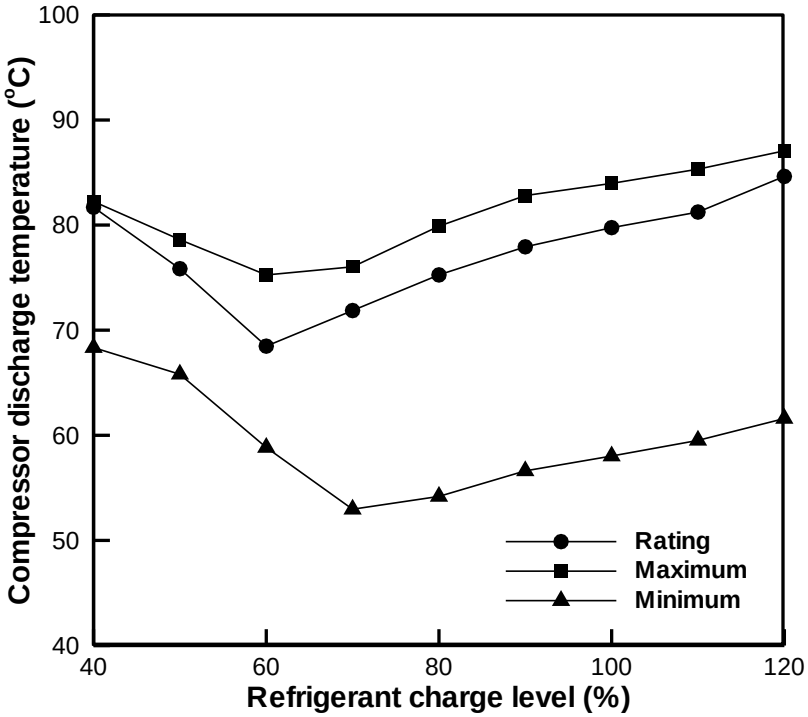

Fig. 3.10 Charge level versus compressor discharge temperature

evaporating pressure decreases and DSH increases rapidly as charge level decreases and both changes reduce density and mass flow rate of refrigerant. At charge level higher than 60% DSH is kept at 5K but evaporating pressure slightly decreases as charge level gets higher so the density and the mass flow rate shows similar behavior. In Fig. 3.10, compressor discharge temperature is shown. When leakage happens, it decreases until the charge level reduces to a point where EEV opening becomes maximum. However, at low charge level, discharge temperature is high because suction DSH is also high at this point thereby increase the superheat at the discharge point.

3.3.2 Detection of refrigerant leakage amount

As mentioned in the section 1.2.2, the detection method usually utilizes DSH and DSC as important indices. From the description of the system with respect to charge level from section 3.4.1., they can be a strong index. Unfortunately, the residential heat pump measures limited points of the system and with the given temperature information, DSH and DSC are hard to obtain. For this reason, refrigerant leakage needs to be detected using the given data. The temperature difference between the midpoint and air inlet at each heat exchanger is considered. Fig. 3.11 shows the temperature difference between

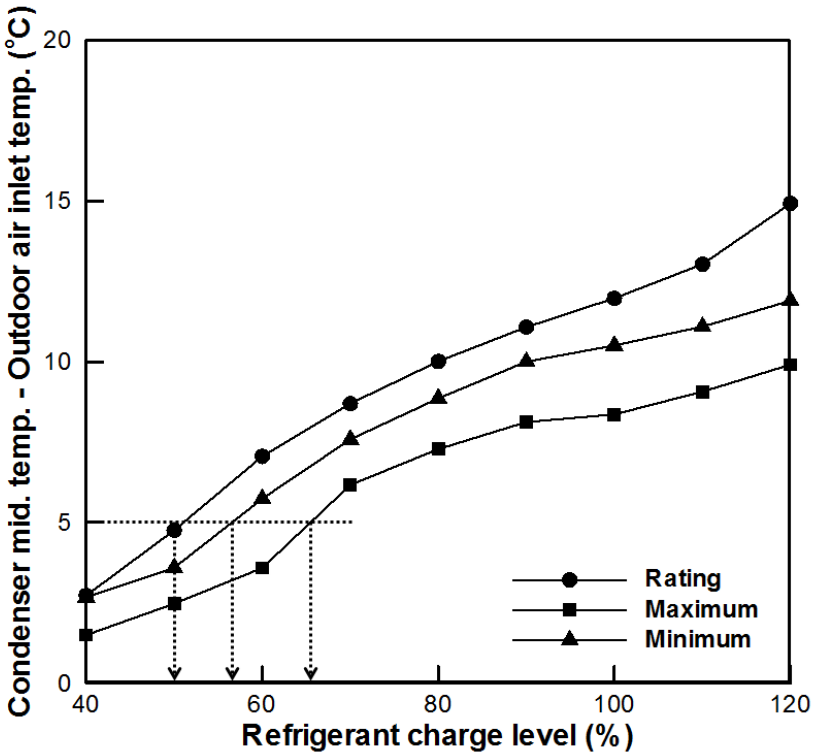

Fig. 3.11 Charge level versus temperature difference at condenser

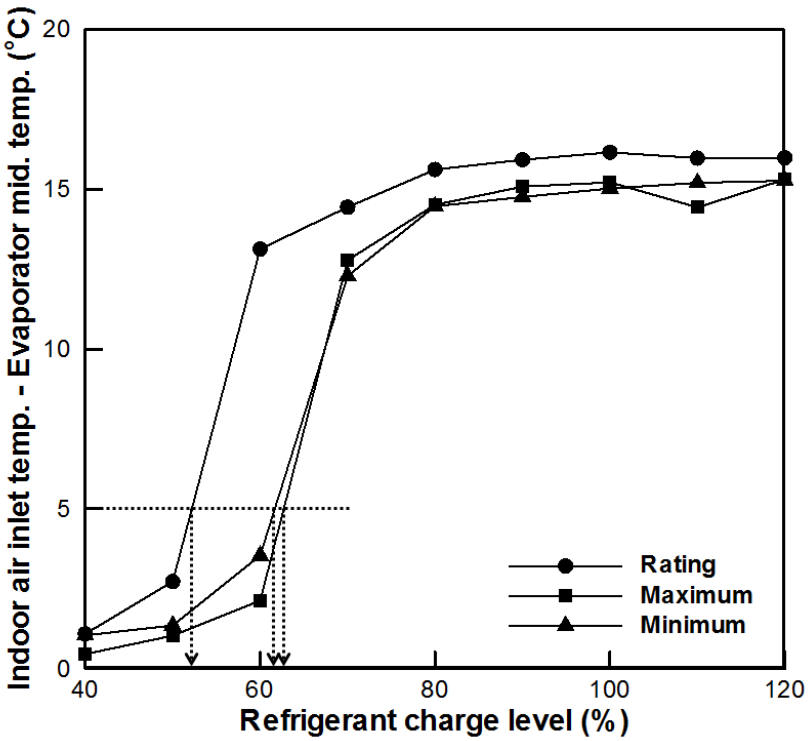

Fig. 3.12 Charge level versus temperature difference at evaporator

the midpoint of the condenser and outdoor air inlet. Fig. 3.12 shows the temperature difference between the indoor air inlet and the midpoint at the evaporator. The temperature difference tends to decrease as charge level goes down. Therefore, a reference temperature value can be set to judge the leakage. When the reference temperature is considered to be 5˚C at condenser in Fig 3.11, charge level is judged around 51% at the rating temperature condition. Similarly, charge level at the maximum and minimum conditions are judged at 65% and 56% respectively. If reference temperature is also considered as 5˚C at evaporator in Fig. 3.12, charge level is detected at 52%, 63% and 62% for each temperature conditions. The leakage detection with the temperature difference is possible on both sides but evaporator side has more advantage. To evaluate the sensitivity of this method using at each exchanger, the slope of the temperature difference and charge level is calculated in Eq. 3.7.

$$Sensitivity\ \ [℃\ \ \%^{-1}] = \frac{\Delta\ temperature\ \ difference}{\Delta\ \ charge\ \ level} \tag{3.7}$$

The sensitivity at condenser side is almost constant throughout the charge level and the average sensitivity is about 0.13˚C $\%^{-1}$. However, the sensitivity at evaporator shows a different trend. The trend is divided into two different parts. In case of the rating temperature condition, the slope is small at charge

level larger than 70% and it is around 0.03˚C $\%^{-1}$. At this range, the temperature difference hardly changes with respect to charge level. Thereby, the temperature difference at condenser is more sensitive at high charge level. On the other hand, in the case of charge level between 50% and 60%, the sensitivity become sharp and it becomes 1.04˚C $\%^{-1}$. It is much higher compared with the sensitivity at condenser at the same range. In case of the other two temperature conditions, sensitivities become the highest between 60% and 70%. Therefore, using the temperature difference at evaporator is more reliable for the detection of leakage amount than that at the condenser. To explain such difference, the temperature distributions at each heat exchanger are investigated. From the modeling, Fig. 3.13 and 3.14 are obtained. The normalized position of these graphs is defined as the ratio of the length of the current position and the inlet to the length of entire evaporator pipe. The normalized position of 0 means inlet side and 1 means outlet side. Fig. 3.13 shows the temperature distribution at condenser at normal condition (charge amount of 1000 g) and a leaked condition (charge amount of 500 g). As explained before, the condensing temperature is higher at the larger charge amount condition. In Fig. 3.13, the temperature installed in the system, which measures the midpoint of the refrigerant side of the condenser, is the same as condensing temperature at any charge amount condition. Since the air inlet temperature does not change, the

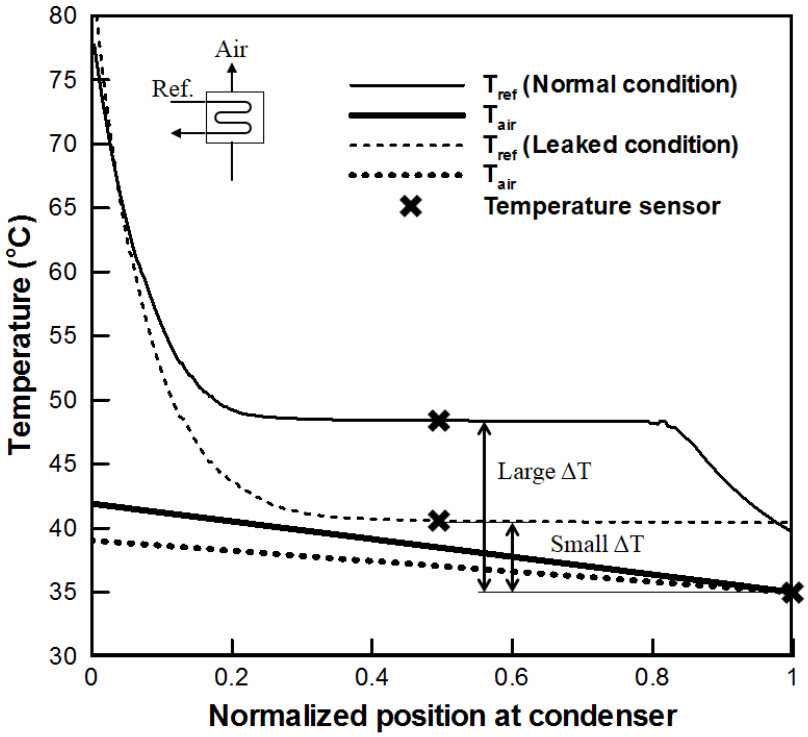

Fig. 3.13 Temperature distribution at condenser (modeling)

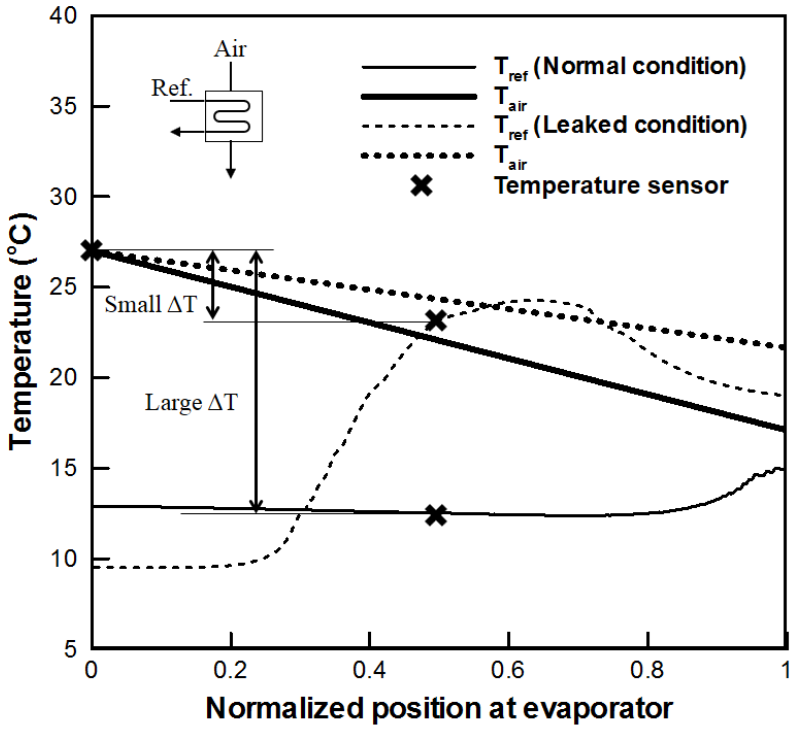

Fig. 3.14 Temperature distribution at evaporator (modeling)

temperature difference between condenser midpoint and the outdoor inlet is always larger as charge level increases. The sensitivity in Eq. 3.7 is nearly constant at condenser because the increment rate of condensing temperature is almost constant. Fig. 3.14 represent the temperature distribution at the evaporator. Similar to Fig. 3.13, evaporating temperature at leaked condition is usually smaller than that in normal condition. However, the midpoint temperature at evaporator is not always the same as evaporating pressure. When the system has enough refrigerant, DSH is in the controllable range. Thus, it remains at 5 K and the superheat state only appears to be on the outlet side of the evaporator. When leakage occurs, DSH becomes higher than the target value and the volume taken by superheated state becomes more than half of evaporator volume. This is because the state of the condenser is at two-phase instead of the subcooled state, so the vapor quality at evaporator inlet also increases. In this case, early evaporation occurs and the refrigerant at midpoint becomes a superheated state. The temperature at this point increases rapidly closer to indoor air inlet temperature. For this reason, the temperature difference between the evaporator midpoint and the indoor air inlet becomes low as leaked condition.

With detailed analysis of the detection method, it concludes that the temperature difference at evaporator have more advantage because it has higher

sensitivity (Eq. 3.7) compare with that at the condenser. The leak detection method, which judges refrigerant charge level based on temperature difference at the evaporator, can have two possible counterexamples that might make this method suspicious. One is the small temperature difference at normal condition and the other is large temperature difference at the leaked condition. However, both situations are not likely to happen. First, at normal condition, the minimum temperature difference must be larger than the DSH. The temperature at air inlet point is always larger than evaporator outlet temperature and if DSH value is larger than 5 K, the temperature difference at evaporator never becomes lower than this value, which proves that the first counterexample never will happen. Second, at the leaked condition, there could be many reasons that could make the temperature difference large, such as reduced fan speed and evaporator fouling, which hinders heat exchange process. However, the detection method is highly related to EEV opening. When refrigerant leakage occurs, the EEV opening becomes larger. If it keeps leaking, it will meet its limit at some point. Until this point, it is not easy to detect leakage but at the EEV fully-opened state the drop of temperature difference is inevitable.

The method in this study can be applied to other systems in the same way with slightly modified detection level. If the different type of refrigerant is used, the absolute value of charge detection level might be changed, but temperature

drop will still occur. In case of a size of the system, the performance and absolute amount of refrigerant charge will also change. The size factor can be normalized by the definition of charge level in Eq. 3.4.

3.4 Advanced detection method with EEV control

The detection method of refrigerant leakage amount with the temperature difference at the evaporator, which is explained in section 3.4.2, can be applied universally but it has the major drawback that the range of detection level is between 52~63%. At this point, both capacity and COP reduces from 40 to 50%. This is a significant performance drop and more sensitive method is required. It should detect refrigerant leakage amount before its charge level drops from 70 to 80%. There are two possible scenarios. One is to change the location of the temperature sensor and the other is to regulate EEV opening.

The temperature sensor is attached to the midpoint of the evaporator but the position can be changed either closer to inlet or outlet. The temperature difference between evaporator midpoint and indoor air inlet sharply reduces when the refrigerant state at measuring point becomes superheated phase. If the sensor position gets closer to the inlet of the evaporator, it is moving toward the location where the refrigerant is at the two-phase state and the detection becomes harder. In contrast, locating the sensor closer to the outlet of the evaporator tends to make detection more sensitive because superheated refrigerant is more likely to be found at the outlet of the evaporator. However, from Fig. 3.15, the temperature at the outlet side of the evaporator is not always the highest compared with that at the inlet side. At the charge level larger than

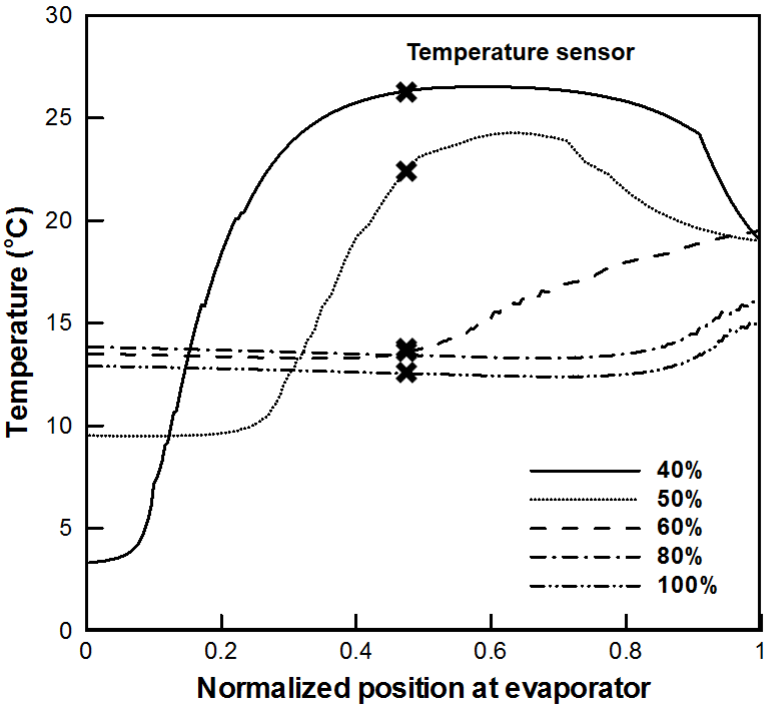

Fig. 3.15 Temperature distribution at evaporator at different charge levels (modeling)

60%, the temperature at evaporator outlet is generally larger than any other point. On the contrary, at charge level lower than 60%, the temperature is the highest at around the normalized position around 0.6. The reason for this is explained in Fig. 3.16. At normal charge condition, the temperature of air keeps decrease as it loses heat from the refrigerant. On the other hand, At leaked condition, the reverse heat transfer occurs partially at the outlet side of the evaporator that the temperature of air increases as it passes the refrigerant. It makes the temperature high at the midpoint and moving the location of the temperature sensor to the outlet is not a reasonable solution. It is because locating the temperature sensor at the highest temperature position tends to decrease the temperature difference between the indoor air inlet and evaporator midpoint. Consequently, the location of the temperature sensors is better to stay at the middle point. In addition, although this experiment is limited to cooling mode, when considering a heat pump system with heating and cooling, installing temperature sensor at the middle position has an advantage. Whether it operates in heating or cooling mode, flow direction changes, but the temperature measuring point at the middle of the heat exchanger can cover both situations.

The other possible solution is to adjust EEV opening on purpose. From previous discussions, two important factors to detect refrigerant leakage are

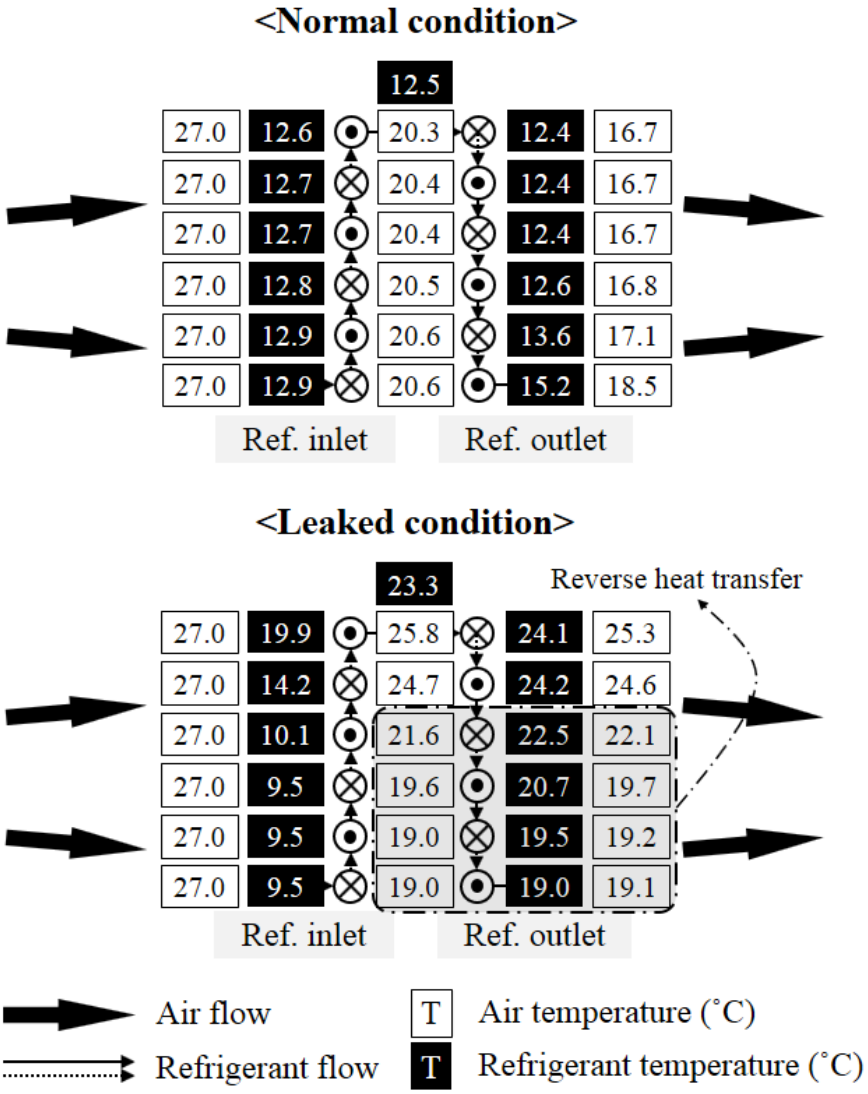

Fig. 3.16 Temperature distribution at evaporator at a normal and a leaked condition (modeling)

revealed. The temperature difference at evaporator sharply decrease when EEV opening reaches its maximum and the state of evaporator midpoint needs to be at the superheated region. Thus, for sensitive detection, the EEV opening is intentionally lowered to force the DSH increase. With the increase of DSH, a volume taken by superheated region at the evaporator rises and if the state at midpoint becomes the superheated state, the detection will more sensitive. Fig. 3.17 shows the flow chart of the advanced detection method. When the system is in normal operation, charge level around 50% is easily detected by the existing method. If the temperature difference value does not drop below 5K, the opening of EEV decreases slightly (5% in this case) on purpose. When the midpoint becomes the superheated state, the temperature difference will drop sharply and by reading the EEV opening, charge level can be judged. To prove this hypothesis, the experiment at each temperature condition but with half of its opening is conducted. Also, the modeling of the heat pump is done for reduced opening conditions. The results are discussed in the following section.

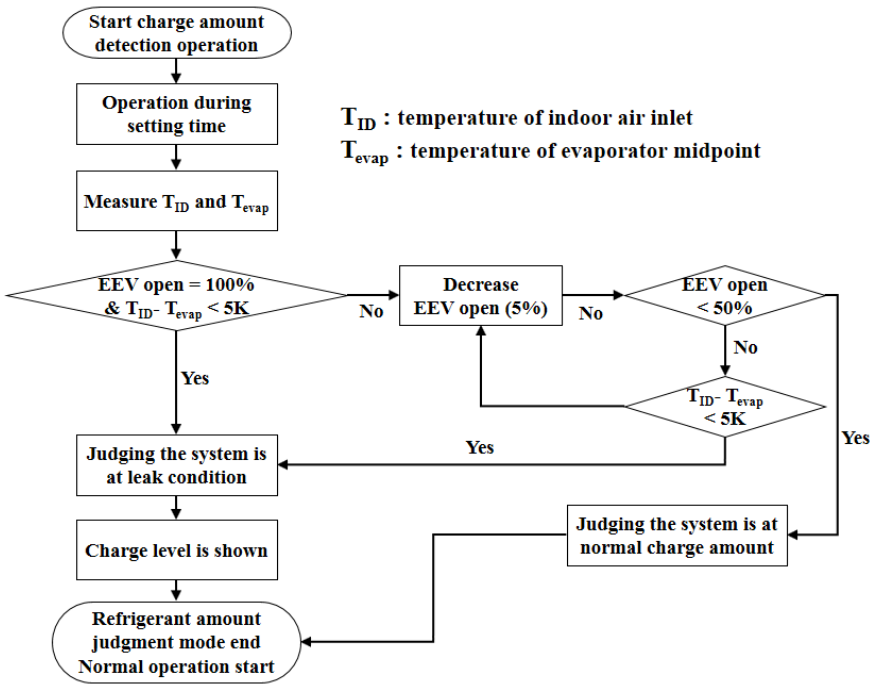

Fig. 3.17 Flow chart of detection method with temperature difference at evaporator and EEV control

3.5 Results and discussion of the advanced method

As expected, from the previous section, decrease in EEV opening make the refrigerant leakage amount detection more sensitive. In Fig. 3.18, the temperature difference between the indoor air inlet and evaporator midpoint at different EEV opening limit condition is shown. The temperature difference at lower EEV opening limit condition becomes lower than 5K at the high charge level condition. In other words, the detection of charge leakage amount is done faster than before. For both modeling and experiment results shows this trend. For the experiment, at the condition where EEV opening limit is 100%, the charge level is 52% when the temperature difference is set at 5K. When the EEV opening limit becomes 50%, charge level becomes 75%. The similar trend is shown in the modeling result. It seems that this method is applicable to any charge level.

However, this method also has limitation. Fig. 3.19 shows the compressor discharge temperature at different charge level and EEV opening limit conditions. Most heat pumps have the upper temperature limitation because lubricant behaves abnormally when the temperature becomes extremely high. By applying EEV opening control to the system, the compressor discharge temperature becomes high. The effect of EEV opening decrease makes suction DSH high, thereby, the discharge DSH and discharge temperature become also

high. From Fig. 3.19, the discharge temperature is higher at a lower EEV opening condition. This shows why it has lower boundary of EEV limit (50%) in Fig. 3.17. The limiting temperature for compressor discharge point in this system is around 110˚C. For this reason, the charge level for detection also has limitation. In this study, it is concluded that this method can detect refrigerant charge level up to 80%.

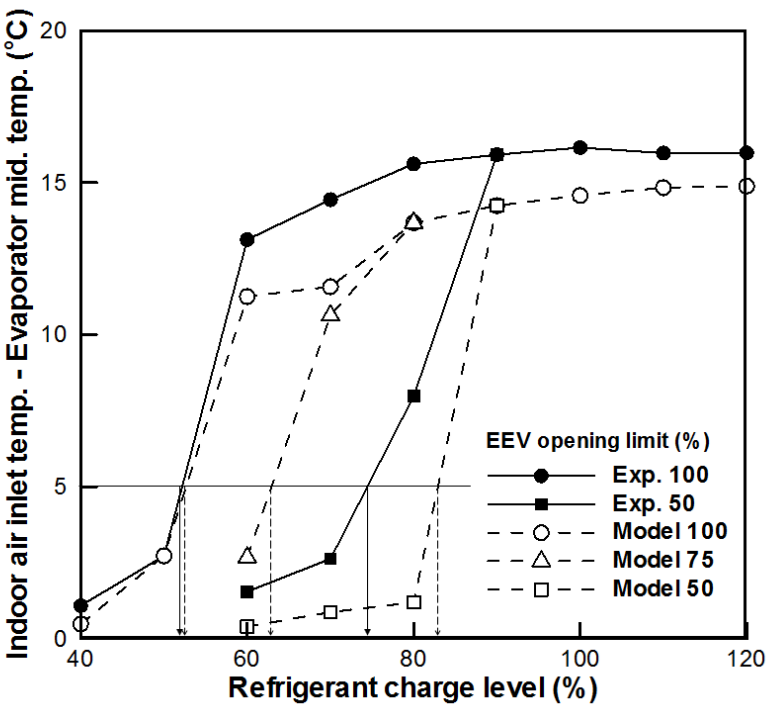

Fig. 3.18 Charge level versus temperature difference at evaporator with different opening limit (rating condition)

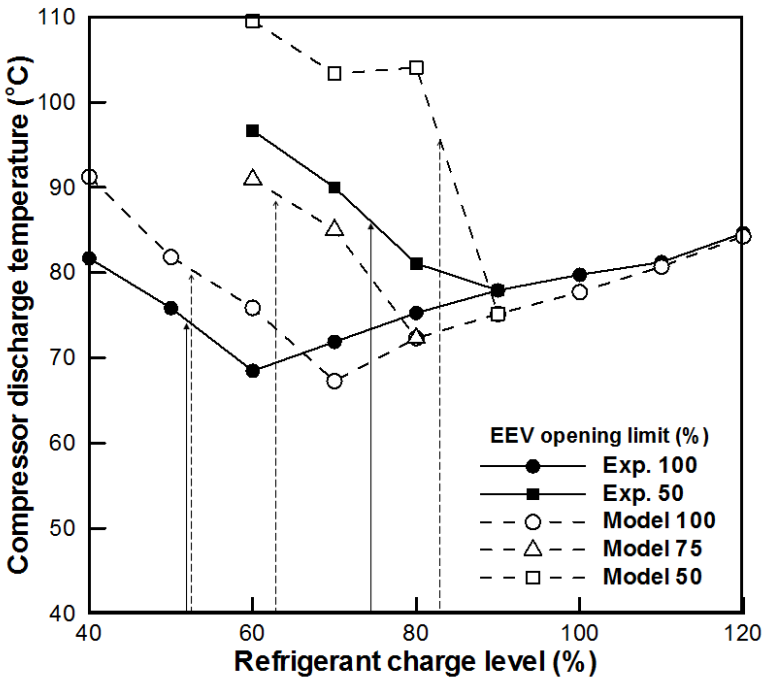

Fig. 3.19 Charge level versus compressor discharge temperature with different opening limit (rating condition)

3.6 Summary

The previous studies suggest DSH and DSC as a useful factor in refrigerant leakage detection. However, the DSH and DSC are hard to obtain in a residential heat pump system due to the lack of sensor installation. In this chapter, the detection method of refrigerant leakage amount is proposed with the temperature difference between the indoor air inlet and the midpoint of the evaporator. The experiment is conducted at three different cooling temperature conditions and various charge amount conditions. The system performance and characteristic with respect to charge amount are illustrated. The detail of the detection method is also explained by both experiment and modeling data. The method is very simple and can be directly applied to systems with different refrigerant or size. However, the detection charge level was around 50 to 60%, which is not satisfactory because the performance at this level already dropped significantly. Thus, the more sensitive detection method is required which can detect charge level at around at 70~80%. Two possible methods are considered which are moving the temperature sensor to outlet side and regulating EEV opening. Through the temperature distribution analysis, it is concluded that the location of the temperature is better to remain at the midpoint. Thereby, the method which adjusts EEV opening was verified with experiment and modeling. With the detection method with EEV control, the detection of refrigerant charge

level increase to 80% which was our objective. Theoretically, a more sensitive detection (charge level of 80%) is possible but it is limited due compressor discharge temperature.

Chapter 4. The detection method of refrigerant leakage amount for in commercial heat pump systems

4.1 Introduction

This chapter treats the method for refrigerant leakage amount detection in commercial heat pump system. From the previous chapter, the temperature difference at evaporator is suggested as a representative value for refrigerant charge level detection. The detection range of this method is between charge level from 50 to 80%. However, a commercial heat pump system requires more sensitive and accurate detection than a residential system. The residential heat pump is expected to have similar installation environment, which means the number of the indoor and outdoor unit, pipe length and air condition is expected to be at the similar range. However, installation condition of the commercial system varies because the number of the indoor and outdoor unit, pipe length and air conditions change largely depending on the installation site. Moreover, commercial systems generally have more control variables because most systems use more complex cycle and the schematic of the system is complicated.

This makes the commercial system more fragile to the refrigerant charge amount.

The previous researches about refrigerant leakage amount are mostly based on the DSH and DSC. The most accurate method until now is from Kim and Braun (2013). They showed the usefulness of the virtual refrigerant charge sensor, which utilizes DSH and DSC, and the overall root mean square (RMS) error was 3.8%. However, this work is constrained to the system with thermal expansion valves or a fixed orifice. Moreover, without tuned parameters, the RMS error increases to 13.9%.

The main goal of this study is to propose a sensitive and accurate method to detect charge level in commercial heat pump systems with EEVs. Fortunately, the number of sensors installed in the commercial system is larger than that in the residential system. The suggested method is based on the temperature distribution at the condenser and outdoor air side. It is accurate and shows linear characteristic over the wide range of refrigerant charge level from 70 to 120%.

4.2 Experimental setup and condition

4.2.1 Commercial heat pump setup and experimental condition

One of the commercial heat pump system with nominal capacity of 30 kW was selected for experiment. Fig. 4.1 shows the image of indoor and outdoor unit of the chosen heat pump. Two indoor units and one outdoor unit were installed to match the capacity between evaporator and condenser. Similar to residential heat pump, it has a variable-speed compressor with scroll type cylinder and EEV (multiple indoor units). Fig. 4.2 displays the schematic of the experiment setup. Accumulator, compressor, oil separator and condenser exist at outdoor unit. Evaporator and EEV is at the indoor unit. The system is installed in the same conditioned chamber that was used from residential heat pump. Thereby, the specification of the chamber is also the same as explained in section 3.2

The heat pump system in the experiment relatively has many sensors. The temperature sensors are installed at the indoor and outdoor air side, accumulator inlet, compressor outlet, condenser inlet and outlet, liquid line and the inlet and outlet of each evaporator. In addition, pressure at the accumulator inlet and compressor outlet is measured. The installed sensors are shown as black circles.

(a) Indoor unit

(b) Outdoor unit

Fig. 4.1 Commercial air heat pump (target model)

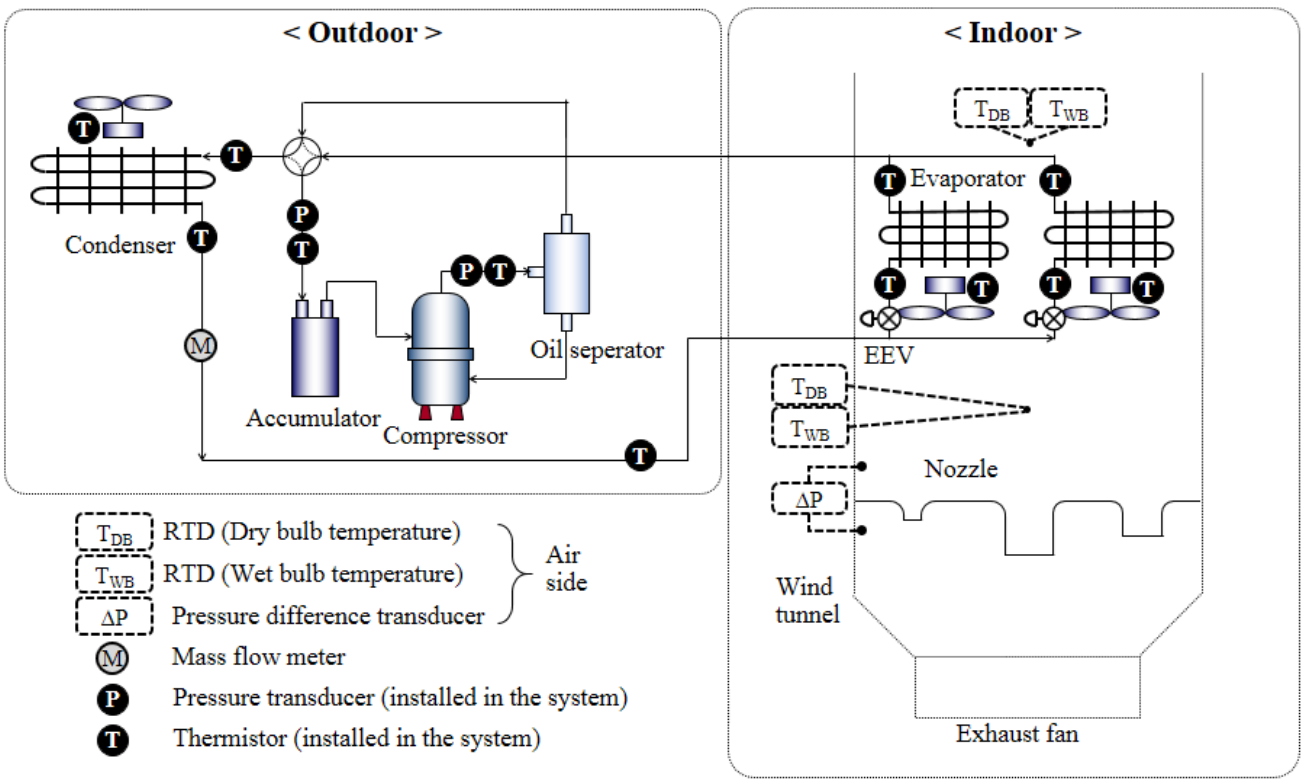

Fig. 4.2 Schematic of experiment setup (commercial heat pump)

The mass flow meter is expensive compared with pressure and temperature sensors so it is installed separately and the gray circle presents it. The specification of the sensors is summarized in Table 4.1.

The component information and experiment condition are shown in Table 2.2 and 2.4 respectively. The initial charge of lubricant is 3.3 kg and the charge amount is changed from 6 to 11 kg. Similar to the residential heat pump, DSH is kept at the fixed value and it is decided to 5, 10 and 15 K in order to validate the detection method at the various condition. According to ANSI/AHRI Standard 1230 (2010), four different air conditions are selected for commercial system. The compressor speed is chosen to be either 60 or 100 Hz. The data are monitored by Labview and are recorded every two seconds after the system reached a steady-state.

4.2.2 Data reduction and uncertainty analysis

The capacity and COP is calculated from Eqs. 3.1 and 3.2, respectively. The uncertainties in rating condition are shown in Table 4.2. The total error of cooling capacity is 5.21% and that of COP is 5.22% respectively on 95% confidence level. The uncertainty in the COP less than 10%, which satisfies ASHRAE Guideline 2 (2010)

Table 4.1 Specifications of measurement instruments

Mass flow meter (Refrigerant side)	
Model	Oval, CN015C-SS-200K
Type	Coriolis
Range	0~200 g/s
Accuracy	±0.1% F.S.
Thermistor (installed in the system - Refrigerant side)	
Model	MITSUBISHI Materials, ACD-45
Range	-30 ~ 130˚C
Accuracy	±0.7˚C
Resistance Temperature Detector (Air side)	
Model	Netsushin, NR-351(PT 100Ω)
Range	-200 ~ 250˚C
Accuracy	(0.15+0.002|T|) ˚C

Table 4.1 Specifications of measurement instruments (continued)

Absolute pressure transducer (Refrigerant side)	
Model	KELLER PA-21Y
Range	0~5000 kPa, 0~6000 kPa
Accuracy	±0.25% F.S.
Differential pressure transducer (Air side)	
Model	Yokogawa, EJA-110A
Range	0~100 mmAq
Accuracy	±0.2% F.S.
Power meter	
Model	Yokogawa, WT 1600
Range	0~12,000 W
Accuracy	±0.1% of reading + 0.05% of range

Table 4.2 Uncertainty analysis at rating condition

Measurements	**Fixed error**	**Random error**	**Total error**
Pressure transducer (condenser side)	0.64%	0.39%	0.75%
Pressure transducer (evaporator side)	1.69%	0.33%	1.72%
Dry bulb air inlet temperature (RTD)	0.20 K	0.03 K	0.21 K
Wet bulb air inlet temperature (RTD)	0.19 K	0.10 K	0.21 K
Dry bulb air outlet temperature (RTD)	0.18 K	0.04 K	0.19 K
Wet bulb air outlet temperature (RTD)	0.18 K	0.06 K	0.19 K
Thermistor	0.70 K	0.26 K	0.75 K
Mass flow rate (refrigerant)	0.17%	0.86%	0.88%
Mass flow rate (air)	3.00%	0.52%	3.05%
Power consumption	0.39%	0.34%	0.52%
Cooling capacity	5.21%	1.75%	5.49%
COP	5.22%	1.78%	5.52%

4.3 Results and discussion

4.3.1 The temperature difference at condenser

In this section, the performance variation with respect to charge level is treated because the trend of the system is very similar to those in residential heat pump system. The optimal charge amount of commercial heat pump system is decided to 9 kg from the experiment. In order to find the reasonable index for charge level detection, the amount of the refrigerant in each component was obtained from the modeling in Fig. 4.3. This chart shows the refrigerant amount of each component at refrigerant amount of the system from 7 to 10 kg. Clearly, the most amount of refrigerant exists in the condenser. It takes about 57 to 65% of the total charge amount in the system. Moreover, the variation of the charge amount with respect to the charge level is also the largest at the condenser. That is to say, condenser is the most important component in the heat pump system when the charge amount is concerned. It is easily explained with refrigerant distribution at heat exchangers in Fig. 4.4. The portion of the liquid refrigerant is high at condenser and the density of liquid is tens or hundreds of times larger compare with that of vapor. For this reason, when refrigerant amount increases, majority of them enters into the condenser.

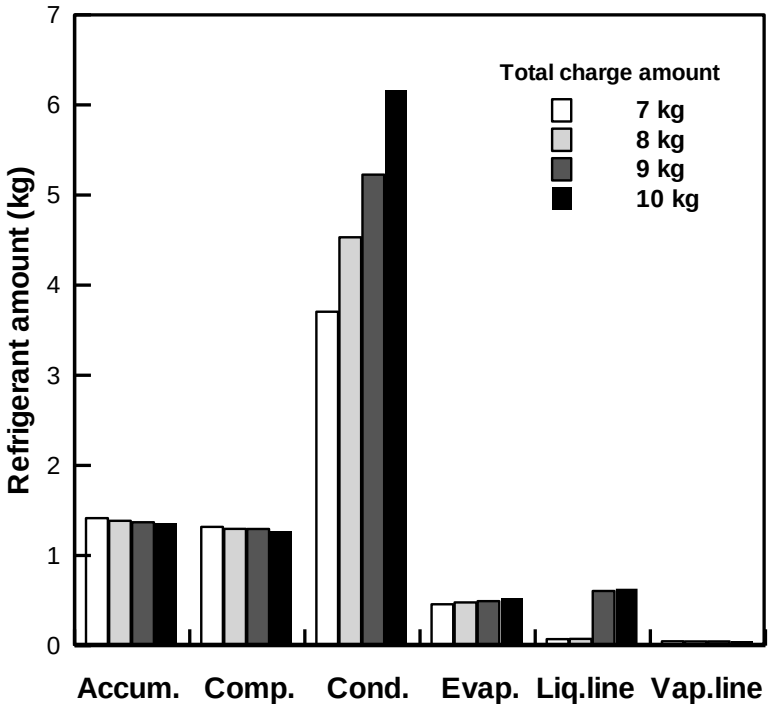

Fig. 4.3 Refrigerant charge amount at each component from the modeling for various charge amount at rating condition (commercial heat pump)

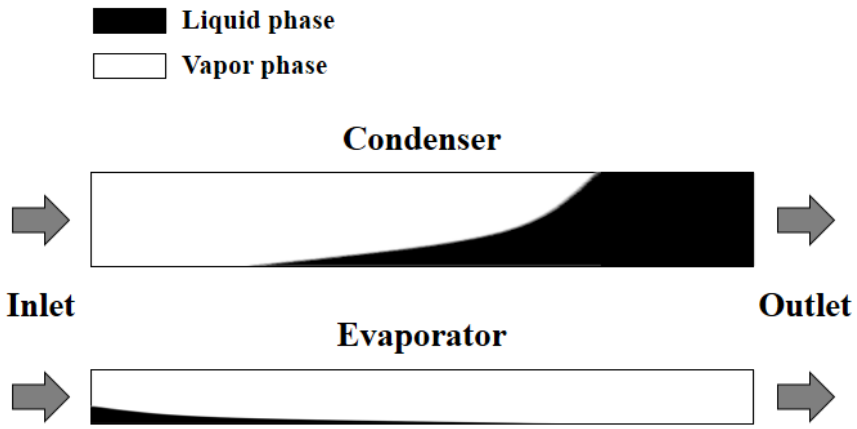

Fig. 4.4 Refrigerant distribution at heat exchangers

Therefore, change at condenser side need to be investigated. Fig. 4.5 represents the change of condensing pressure to charge level at different temperature and compressor rotational speed conditions. It seems that the change of condensing pressure shows linear behavior and it is easily guessed that the condensing pressure also assumed to have linear correlation with charge level. The absolute pressure value is large at high outdoor air temperature condition. Thereby, the difference between condensing temperature and outdoor air inlet temperature can be a representative index for charge level detection. In Fig. 4.6, the temperature difference at condenser with respect to charge level is shown at various conditions. Unfortunately, this is not a good index because the data is too dispersed thereby a better index is required.

4.3.2 Log mean temperature difference (LMTD) at condenser

Instead of the difference between condensing temperature and the temperature of the outdoor air inlet, log mean temperature difference (LMTD) at condenser is calculated. Fig. 4.7 shows the temperature distribution at condenser. From the sensors installed in the system, it is possible to get the temperature at condenser inlet and outlet and outdoor air inlet. The condensing temperature is also can be obtained from the pressure value. Then air

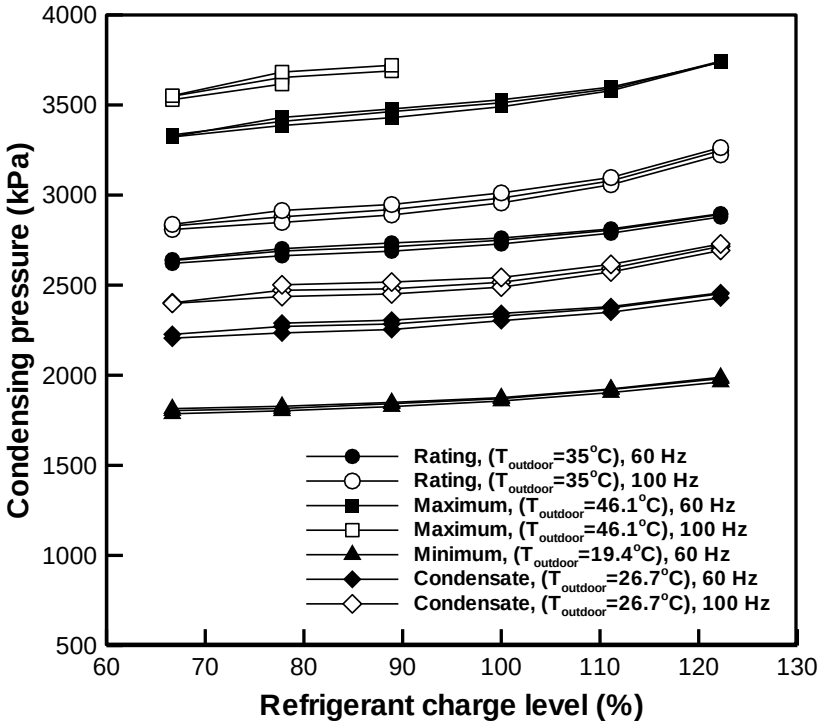

Fig. 4.5 Charge level versus condensing pressure at various conditions

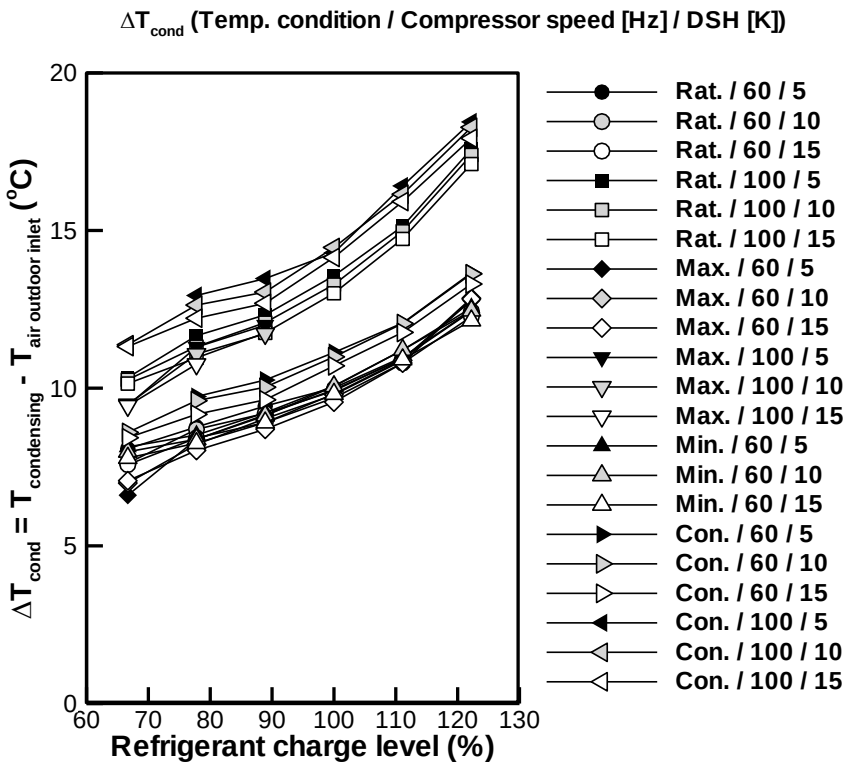

Fig. 4.6 Charge level versus temperature difference at condenser for various conditions

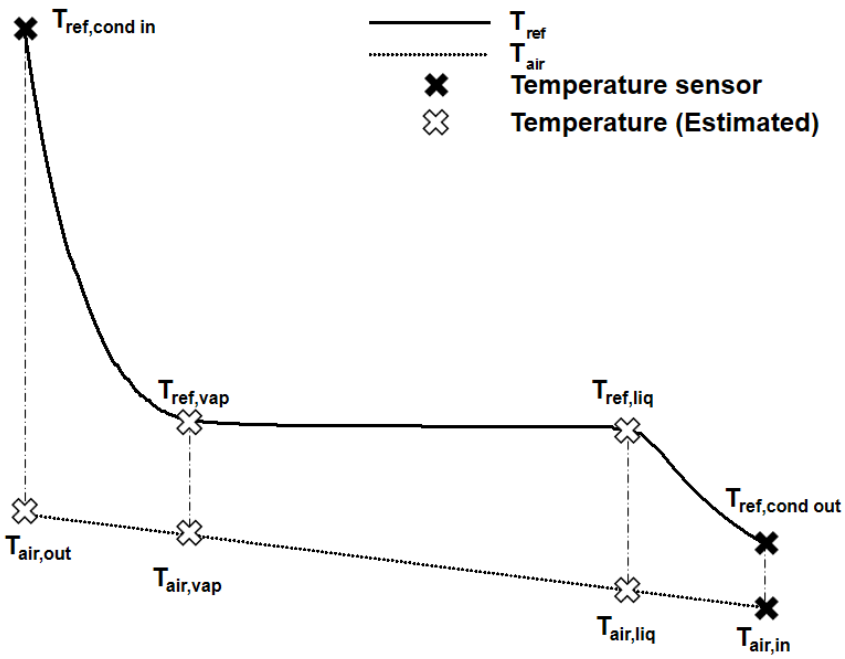

Fig. 4.7 Temperature distribution at condenser

temperature at the point where refrigerant state is saturated liquid and saturated vapor ($T_{air,liq}$ and $T_{air,vap}$) can be calculated from the heat balance of the refrigerant and air side with Eqs. 4.1 to 4.4.

$$Q_{SC} = \dot{m}_{ref} \cdot \left(i_{ref,sat.liq} - i_{ref,cond,out}\right) = \dot{m}_{air} C_{p,air} \cdot (T_{air,liq} - T_{air,in}) \quad (4.1)$$

$$Q_{TP} = \dot{m}_{ref} \cdot \left(i_{ref,vap.liq} - i_{ref,liq}\right) = \dot{m}_{air} C_{p,air} \cdot (T_{air,vap} - T_{air,liq}) \quad (4.2)$$

$$\dot{m}_{ref} = \rho_{comp,in} V_{displacement} \omega_{compressor} \quad (4.3)$$

$$\rho_{comp,in} = f(P_{comp,in}, T_{comp,in}) \quad (4.4)$$

The volume displacement and the mass flow rate of air need to be known previously because these are not obtained from the sensor information. Once $T_{air,liq}$ and $T_{air,vap}$ are calculated, the log mean temperature difference (LMTD) at the two-phase region of condenser side can be obtained from Eq. 4.5.

$$LMTD = \frac{[(T_{ref,vap} - T_{air,vap}) - (T_{ref,liq} - T_{air,liq})]}{\ln[(T_{ref,vap} - T_{air,vap})/(T_{ref,liq} - T_{air,liq})]} \quad (4.5)$$

The change in LMTD for charge level is shown Fig. 4.8. The data is largely divided into two groups according to the compressor rotational speed. The

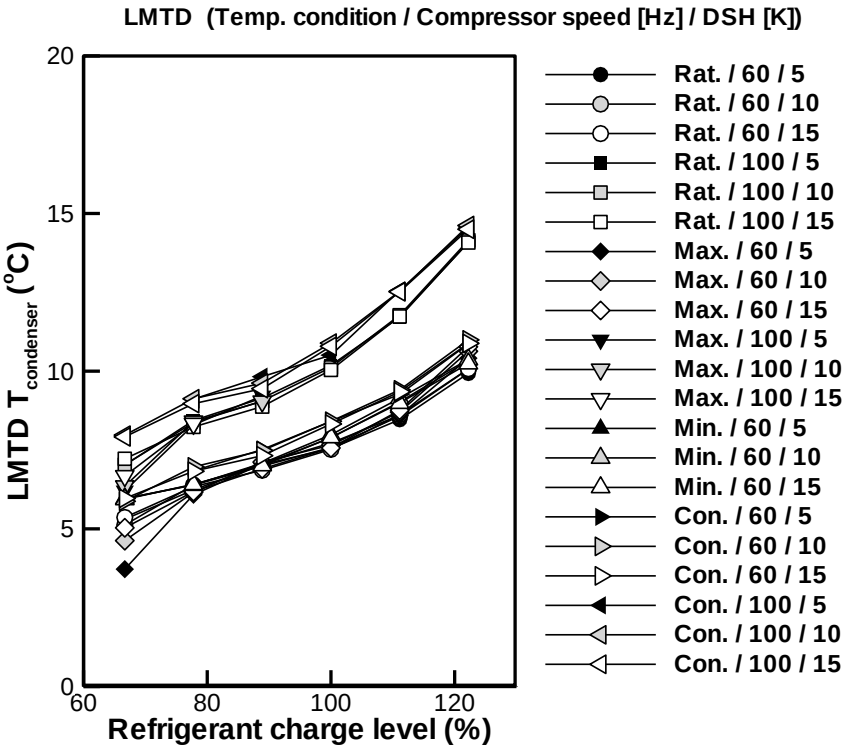

Fig. 4.8 Charge level versus LMTD at condenser for various conditions

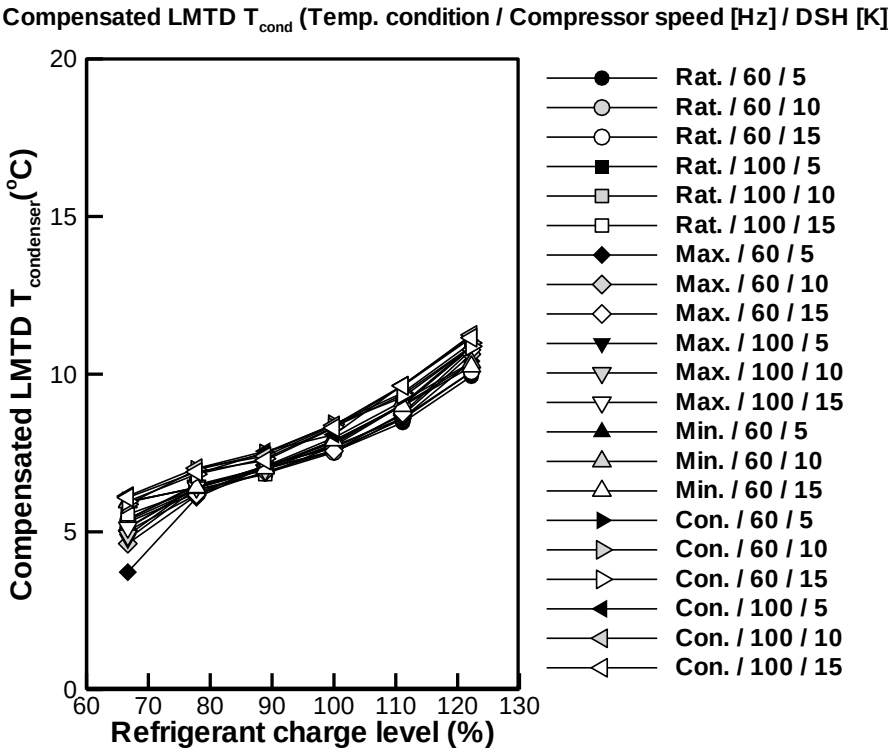

Fig. 4.9 Charge level versus compensated LMTD at condenser for various conditions

average LMTD at optimal point is 7.8 and 10.4 K when the rotational speed of compressor is at 60 and 100 Hz respectively. By compensating the LMTD values for the compressor rotational speed, experiment data are gathered at a proper range in Fig 4.9. The compensated LMTD at condenser shows linearity over the charge level between 70 to 120%. Fig 4.10 compares the actual and estimated refrigerant charge amount in the system. Most of the data are within 10% error range and root mean square (RMS) error is 5.9%. The reason for the large deviation at low charge amount (6 kg) is that the method applies to the condition where the state of condenser outlet is at subcooled state. However, when the system charge level becomes lower than 70%, DSC become zero because condenser outlet is at two-phase state. Since the quality of the refrigerant at two-phase condition is hard to obtain, the $T_{air,liq}$ and $T_{air,vap}$ become inaccurate. Therefore, this method can be applied where the condenser outlet is at subcooled state.

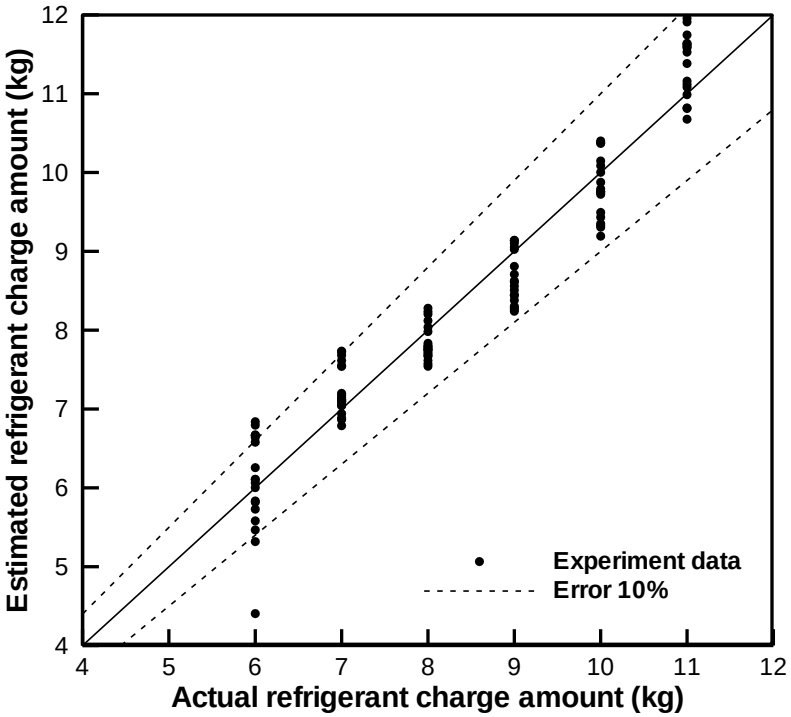

Fig. 4.10 Actual and estimated refrigerant charge amount

4.4 Summary

In order to detect the charge level of the commercial heat pump, a compensated LMTD is calculated from the system information. With the modeling, it is revealed that the condenser side has the large charge amount of the system, and it varies highly with respect to the charge level. Moreover, the change of the condensing pressure for charge level shows linear behavior. For this reason, the refrigerant charge amount in the system can be determined with the behavior at condenser side. The temperature distribution of air and refrigerant side is acquired from the heat balance and LMTD at condenser two-phase region is obtained. The LMTD values are divide into groups according to the compressor rotational speed. Therefore, the LMTD values are compensated for the compressor rotational speed. From the compensated LMTD at the condenser, charge amount in the system is predicted with RMS error of 5.9%. However, this method is limited to the charge level over 70% because the condenser outlet state needs to be at subcooled state in order to apply it.

Chapter 5. Concluding remarks

The energy use through HVAC (Heating, Ventilation & Air Conditioning) takes 40% of residential, building and commercial energy use and heat pumps are essential equipment in HVAC. The penetration of heat pump is over 80% in the United State, thereby the maintenance is important. One of the most frequently occurred and costly fault in heat pumps is refrigerant leakage. When leak occurs, first, leak point need to be found and fix it. The location of refrigerant leakage can be easily detected once we have a proper refrigerant detector. After that, charge amount leaked from the system need to be recovered. For this reason, the amount of leaked refrigerant needs to be determined from the system behavior. In order to suggest a proper method for refrigerant leakage amount detection, both modeling and experiment are conducted.

The modeling process of the heat pump system regarding lubricant is treated in Chapter 2. The optimal charge amount in the modeling is largely underpredicted from 10 to 30% compare with experimental results for residential and commercial heat pumps. This difference is mainly due to the lubricant. Most heat pump modeling is done without lubricant because the oil circulation ratio is small compare to the mass flow rate of refrigerant and both heat transfer and pressure drop do not significantly affected by the existence of lubricant. However, the amount of refrigerant dissolved in the lubricant is

significant because refrigerant exists in the form of liquid instead of vapor phase. With the property equations of refrigerant and lubricant mixture, the component and cycle modeling is carried. After the lubricant is considered in the modeling, the results show good matches with experiment. Lubricant clearly is the most important factor in the heat pump modeling especially when charge amount is concerned.

In chapter 3, the detection method of refrigerant leakage amount in the residential heat pump system. For ease of understanding, the charge level is defined as the ratio of the current charge amount to the optimal charge amount in the system. The residential system only have small number of sensors and within this limitation, the current charge level needs to be found as sensitive as possible. The suggested method utilizes the temperature sensor at evaporator side, which are located at the indoor air inlet and evaporator midpoint. At normal charge level condition, the temperature difference at evaporator is usually larger than the 5K because the DSH is larger than 5 K and evaporator midpoint stay at two-phase condition. At leaked condition, the EEV opening reaches maximum so the evaporator midpoint state becomes superheated and the temperature difference at evaporator becomes smaller than 5K. With this principle, charge level from 55 to 65% is judged. With the EEV control method, which intentionally reduces the opening value of EEV, the detection range of

charge level becomes around 80%. Theoretically, a more sensitive detection is possible but it is limited due compressor discharge temperature.

In chapter 4, the different detection method is suggested which can be applied to the commercial system. The importance of the condenser with respect to charge amount is explained. The relationship between the charge level and condensing pressure (or temperature) showed proportional relation. From this fact, the log mean temperature difference at condenser two-phase region is calculated with system variables. The data are divided into groups according to the compressor rotational speed and with the compensated LMTD at condenser charge amount in the system is predicted with RMS error of 5.9%. However, this method is limited to the charge level over 70% because the condenser outlet state needs to be at subcooled state in order to apply it.

Through this study, the two different detection method for refrigerant charge level is suggested and each method is verified with both experiment and modeling data. This study is useful for any air heat pump system because majority of them are suffer from the refrigerant leak problem. In addition, these methods are not intended for future use, but can be applied immediately to existing systems.

References

ANSI/AMCA 210, 2007. Laboratory methods of testing fans for certified aerodynamic performance rating. Air Movement and Control Association International, Inc., Arlington, IL, U.S.A.

ANSI/AHRI Standard 1230, 2010. Performance Rating of Variable Refrigerant Flow (VRF) Multi-Split Air-Conditioning and Heat Pump Equipment. Arlington, VA, U.S.A.

ASHRAE, 2009. ASHRAE Handbook Fundamentals, Chapter 1. Psychrometrics, Atlanta, GA, U.S.A.

ASHRAE Guideline 2, 2010. Engineering analysis of experimental data. ASHRAE, Atlanta, GA, U.S.A.

ASHRAE, 2014. ASHRAE Handbook Refrigeration, Chapter 12. Lubricants in refrigerant systems, Atlanta, GA, U.S.A.

Bailey, M.B., 1998. System performance characteristics of a helical rotary screw air-cooled chiller operating over a range of refrigerant charge conditions. ASHRAE Transactions. 104, 274-285.

Barnea, D., Shoham. O., Taitel. Y., 1982. Flow pattern transition for downward inclined two phase flow; horizontal to vertical. Chemical Engineering Science. 37(5), 735-740.

Bender, F., Skrypnik. A., Voigt, A., Marcoll, J., Rapp M., 2003. Selective

Detection of HFC and HCFC Refrigerants Using a Surface Acoustic Wave Sensor System. Anal. Chem. 75, 5262-5266.

Biddle, J., 2008. Explaining the spread of residential air conditioning, 1955–1980. Explor. Econ. Hist. 45, 402-423.

Buildings Energy Data Book, 2011. Department Of Energy : https://openei.org/doe-opendata/dataset/buildings-energy-data-book; 2017 [accessed 17.09.18]

Busche, S., Dieterle, F., Kieser, B., Gauglitz, G., 2003. Quantification of binary mixtures of the freones R22 and R134a by surface plasmon resonance. Sensors and Actuators B 89, 192-198.

Butterworth, D., 1969. Note on fully-developed, horizontal, annular two-phase flow. Chemical Engineering Science. 24, 1832-1834.

Casciaro, S., Thome, J., 2001. Thermal performance of flooded evaporators, part 2: Review of void fraction, two-phase pressure drop, and flow pattern studies. ASHRAE Transactions. 107, 919-930.

Cengel, Y.A., 2003. Heat transfer, second ed. Mcgrew-hill, Singapore.

Chen, S.L., Gerner, F.M., Tien, C.L., 1987. General film condensation correlations. Experimental heat transfer. 1, 93-107.

Cheng, L., Ribatski, G., Thome, J., 2008. Two-Phase Flow Patterns and Flow-Pattern Maps: Fundamentals and Applications. Applied Mechanics Reviews.

61. 050802.

Comstock, M.C., Braun, J.E., 1999. Development of analysis tools for the evaluation of fault detection and diagnostics for chillers. ASHRAE Report #4036-3.

Corberán, J.M., Martínez, I.O., Gonzálvez, J., 2008. Charge optimisation study of a reversible water-to-water propane heat pump. Int. J. Refrig. 31, 716-726.

Corberán, J.M., Martínez-Galván, I., Martínez-Ballester, S., Gonzálvez-Maciá, J., Royo-Pastor, R., 2011. Influence of the source and sink temperatures on the optimal refrigerant charge of a water-to-water heat pump. Int. J. Refrig. 34, 881-892.

Cremaschi, L., 2004. Experimental and theoretical investigation of oil retention in vapor compression systems. Ph.D thesis, University of Maryland, U.S.A.

Dieterle, F., Belge, G., Betsch, C., Gauglitz, G., 2002. Quantification of the refrigerants R22 and R134a in mixtures by means of different polymers and reflectometric interference spectroscopy. Anal. Bioanal. Chem. 374, 858-867.

Dittus, F. W., Boelter, L. M. K., 1930. Heat transfer in automobile radiators of the tubular type. The University of California Publications on Engineering 2. 443-461, Reprinted 1985. Int. Commun. Heat Mass. 12, 3-22.

Francis, C.,Maidment, G., Davies, G., 2017. An investigation of refrigerant leakage in commercial refrigeration, . Int. J. Refrig. 74, 12-21.

Gaitonde, U.N., Deshpande, D.D., Sukhatme, S.P., 1978. The thermal conductivity of liquid mixtures. Ind. Eng. Chem. Fundam. 17(4), 321-325.

Ghoubali, R., Byrne, P., Bazantay, F., 2017. Refrigerant charge optimisation for propane heat pump water heaters. Int. J. Refrig. 76, 230-244.

Godbole, P., Tang, C., Ghajar, A., 2011. Comparison of Void Fraction Correlations for Different Flow Patterns in Upward Vertical Two-Phase Flow. Heat tranfer engineering 32(10), 843-860.

Grace, I.N., Datta, D., Tassou, S.A., 2005. Sensitivity of refrigeration system performance to charge levels and parameters for on-line leak detection. Appl. Therm. Eng. 25, 557–566.

Grill, J., Singh, J., 2017. Experimental Analysis of R134a/LPG as Replacement of R134a in a Vapor-Compression Refrigeration System. International Journal of Air-Conditioning and Refrigeration 25(2), 1750015.

Gungor, K., Winterton, R., 1987. Simplified gernaral correlation for saturated flow boiling and comparisons with data, Chemical Engineering Research and Design. 65, 148-156.

Hewitt, N. J., McMullan, J. T., Murphy, N. E., Shafaghian, N. E. 1991. A solublilty equation for R22-oil mixtures, Int. J. Energy Research. 15, 763-768.

Hewitt, N. J., Lemmon, E.W., Huber, M.L., McLinden, M.O., 2013. NIST

Standard Reference Database 23: Reference Fluid Thermodynamic and Transport Properties-REFPROP, Version 9.1. National Institute of Standards and Technology, Standard Reference Data Program: Gaithersburg, MD

Hsiung, J.T., Himmelblau, D.M., 1996. Detection of leaks in a liquid-liquid heat exchanger using passive acoustic noise. Computers chem. Engng. 20(9), 1101-1111.

Hughes, D. W., McMullan, J. T., Mawhinney, K. A., Morgan, R., 1982. Pressure-enthalpy charts for mixtures of oil and refrigerant R12, Int. J. Refrig. 5(4), 199-202.

Hughmark, G.A., 1962. Holdup in gas-liquid flow. Chemical Engineering Progress. 58(4), 62-65.

ISO 5151, 2010. Non-ducted air conditioners and heat pumps - testing and rating for performance. Geneva, Switzerland

Jin, S.,Hrnjak, P., 2016. Refrigerant and lubricant charge in air condition heat exchangers: Experimentally validated model. Int. J. Refrig. 67, 395-407.

Kim, D.H., Park, H.S., Kim, M.S., 2014. The effect of the refrigerant charge amount on single and cascade cycle heat pump systems. Int. J. Refrig. 40, 254-268.

Kim, H.S., Yoon, P.Y., Sa, Y.C., Chung, B.Y., Kim, M.S., 2014. A study on the flow characteristics of refrigerant and oil mixture in compressor suction line.

Int. J. Refrig. 48, 48-59.

Kim, H.S., Kim, M.S., 2015. A Review on Flow Characteristics of Refrigerant and Oil Mixture in a Heat Pump System. International Journal of Air-Conditioning and Refrigeration 23(3), 1530002.

Kim, H.S., Kim, M.S., 2016. A numerical study on the oil retention of R410A and PVE oil mixture in multi heat pump system, Journal of Mechanical Science and Technology 30 (4), 1891~1901.

Kim, J.H., Cho, J.M, Lee, I.H., Lee, J.S., Kim, M.S., 2007. Circulation concentration of CO2/propane mixtures and the effect of their charge on the cooling performance in an air-conditioning system. Int. J. Refrig. 30, 43-49.

Kim, M., Kim, M.S., 2005. Performance investigation of a variable speed vapor compression system for fault detection and diagnosis. Int. J. Refrig. 28, 481–488.

Kim, M., Yoon, S.H., Payne, W.V., Domanski, P.A., 2008. Cooling mode fault detection and diagnosis method for a redidential heat pump, NIST Special Publication 1087

Kim, N., 2017. Optimization of the Water Spray Nozzle, Refrigerant Charge Amount and Expansion Valve Opening for a Unitary Ice Maker Using R-404A. International Journal of Air-Conditioning and Refrigeration 25(3), 1750025.

Kim, W., Braun, J.E., 2012. Extension of a Virtual Refrigerant Charge Sensor. International Refrigeration and Air Conditioning Conference

Kim, W., Braun, J.E., 2013. Performance evaluation of a virtual refrigerant charge sensor. Int. J. Refrig. 36, 1130-1141.

Kim, W., Braun, J.E., 2015. Extension of a virtual refrigerant charge sensor. Int. J. Refrig. 55, 224-235.

Kocyigit, N.,Bulgurcu, H., Lin, C., 2014. Fault diagnosis of a vapor compression refrigeration system with hermetic reciprocating compressor based on p-h diagram. Int. J. Refrig. 45, 44–54.

LeRoy, J.T., Groll, E.A., Braun, J.E., 2000. Evaluating the accuracy of PUREZ in predicting unitary equipment performance. ASHRAE transaction. 106, 200-215.

Li, G., Hu, Y., Chen, H., Shen, L., Li, H., Li, Jiong., Hu, W., 2016. Extending the virtual refrigerant charge sensor (VRC) for variable refrigerant flow (VRF) air conditioning system using data-based analysis methods. Applied Thermal Engineering 93, 908-919.

Li, H., Braun, J.E., 2004. A Methodology for Diagnosing Multiple-Simultaneous Faults in Rooftop Air Conditioners. International Refrigeration and Air Conditioning Conference

Li, H., Braun, J.E., 2004. An Economic Evaluation of Automated Fault

Detection and Diagnosis for Rooftop Air Conditioners. International Refrigeration and Air Conditioning Conference

Li, H., Braun, J.E., 2007. Decoupling features and virtual sensors for diagnosis of faults in vapor compression air conditioners. Int. J. Refrig. 30, 546-564.

Li, H., Braun, J.E., 2009. Development, Evaluation, and Demonstration of a Virtual Refrigerant Charge Sensor, HVAC&R Research 15(1), 117-136.

Li, G., Hu., Y, Chen, H., Shen L., Li, H., Li, J., Hu, W., 2016. Extending the virtual refrigerant charge sensor (VRC) for variable refrigerant flow (VRF) air conditioning system using data-based analysis methods. Applied Thermal Engineering 93, 908–919.

Li, T., Lu, J., Chen, L., He, D., Qiu, X., Li, H., Liu, Z., 2015. Measurement of refrigerant mass distribution within a R290 split air conditioner. Int. J. Refrig. 57, 163-172.

Liu, J., Li, G., Chen, H., Wang, J., Guo, Y., Li, Jiong., 2017. A robust online refrigerant charge fault diagnosis strategy for VRF systems based on virtual sensor technique and PCA-EWMA method. Applied Thermal Engineering 119, 233-243.

Ma, X., Ding, G., Zhang, P.,Han, W.,Kasahara, S.,Yamaguchi, T., 2009. Experimental validation of void fraction models for R410A air conditioners. Int. J. Refrig. 32, 780-790.

Madani, H., Roccatello, E., 2014. A comprehensive study on the important faults in heat pump system during the warranty period. Int. J. Refrig. 48, 19-25.

Marsh, K.N., Kandil, M.E., 2002. Review of thermodynamic properties of refrigerants + lubricant oils. Fluid Phase Equilibria 199, 319-334.

Martı´nez-Galva´n, I.,Gonza´lvez-Macia´, J., Corbera´n, J., Royo-Pastor, R., 2011. Oil type influence on the optimal charge and performance of a propane chiller. Int. J. Refrig. 34, 1000-1007.

Mehendale, S.S., Radermacher, R., 2000. Experimental and Theoretical Investigation of Annular Film Flow Reversal In a Vertical Pipe: Application To Oil Return In Refrigeration Systems, HVAC&R Research 6(1), 55-74.

Mowris, R., Blankenship, A., Jones, E., 2004. Field Measurements of Air Conditioners With and Without TXV's, American Council for an Energy-Efficient Economy, Summer Study Proceedings.

Muller-steinhagen, H., Heck, K., 1986. A Simple Friction Pressure Drop Correlation for Two-Phase Flow in Pipes, Chem. Eng. Process. 20, 297-308.

Peuker, S., 2010, Experimental and analytical investigation of refrigerant and lubricant migration. Ph.D thesis, University of Illinois at Urbana-Champaign, U.S.A.

Radermacher, R., Cremaschi, L., Schwentker R.A., 2006. Modeling of Oil

Retention in the Suction Line and Evaporator of Air-Conditioning Systems, HVAC&R Research 12(1), 35-56.

Rice, C.K, 1987. The effect of void fraction correlation and heat flux assumption on refrigerant charge inventory predictions. ASHRAE transaction. 93(1), 341-367

Rossi, T.M., Braun, J.E., 1997. A Statistical, Rule-Based Fault Detection and Diagnostic Method for Vapor Compression Air Conditioners. HVAC&R Research 3(1), 19-37.

Rossi, T.M., 2004. Unitary air conditioner field performance. International Refrigeration and Air Conditioning Conference.

Rouhani, S.Z., Axelsson, E., 1970. Calculation of void volume fraction in the subcooled and quality boiling regions. Int. J. Heat and Mass transfer. 13, 383-393.

Shen, B., Groll, E.A., 2005a. A Critical Review of the Influence of Lubricants on the Heat Transfer and Pressure Drop of Refrigerants, Part I: Lubricant Influence on Pool and Flow Boiling, HVAC&R Research 11(3), 341-359

Shen, B., Groll, E.A., 2005b. A Critical Review of The Influence of Lubricants on the Heat Transfer and Pressure Drop of Refrigerants—Part II: Lubricant Influence on Condensation and Pressure Drop, HVAC&R Research 11(4), 511-526.

Shen, B., Groll, E.A., 2005. Review Article: A Critical Review of the Influence of Lubricants on the Heat Transfer and Pressure Drop of Refrigerants, Part 1: Lubricant Influence on Pool and Flow Boiling, HVAC&R Research 11(3), 341-359.

Taitel, Y., Dukler, A.E., 1976. A Model for Predicting Flow Regime HorizontaI and Near HorizontaI Gas-liquid Flow, AlChe Journal 22(1), 47-55.

Tang, W., He G., Cai, D., Zhu, Y., Zhang, A., Tian, Q., 2017. The experimental investigation of refrigerant distribution and leaking characteristics of R290 in split type household air conditioner. Applied Thermal Engineering 115, 72–80.

Tassou, S.A., Grace, I.N., 2005. Fault diagnosis and refrigerant leak detection in vapour compression refrigeration systems. Int. J. Refrig. 28, 680-688.

Temple, K.A., 2004, A Performance Based Method to Determine Refrigerant Charge Level in Unitary Air Conditioning and Heat Pump Systems. International Refrigeration and Air Conditioning Conference.

Tesser, R., Musso, E., Di Serio, M., Basile,G., Santacesari,E., 1999. Description of the vapor±liquid equilibrium in binary refrigerant/lubricating oil systems by means of an extended Flory±Huggins model. Journal of Fluorine Chemistry 99, 29-36.

Ursenbacher, T., Wojtan, L., Thome, J., 2004. Interfacial measurements in

stratified types of flow. Part I: New optical measurement technique and dry angle measurements. Int. J. Multiphase Flow. 30, 107-124.

U.S Energy Information Administration, 2012. Annual Energy Review 2011. 54-55.

Wallis, G., 1969. One Dimensional Two-Phase Flow. McGraw-Hill, New York.

Wang, C., Chi, K., 2000. Heat transfer and friction characteristics of plain fin-and-tube heat exchangers, part I: new experimental data. Int. J. Heat and Mass transfer. 43, 2681-2691.

Wang, C., Chi, K., Chang, C., 2000. Heat transfer and friction characteristics of plain fin-and- tube heat exchangers, part II: Correlation. Int. J. Heat and Mass transfer. 43, 2693-2700.

Wojtan, L., Ursenbacher, T., Thome, J., 2004. Interfacial measurements in stratified types of flow. Part II: Measurements for R-22 and R-410A. Int. J. Multiphase Flow. 30, 125-137.

Wojtan, L., Ursenbacher, T. Thome, J., 2005. Investigation of flow boiling in horizontal tubes: Part I—A new diabatic two-phase flow pattern map. Int. J. Heat and Mass transfer. 48, 2955-2969.

Woldesemayat, M.A., Ghajar, A.J., 2007. Comparison of void fraction correlations for different flow patterns in horizontal and upward inclined pipes. Int. J. Multiphase Flow. 33, 347–370.

Yoo J.W., Hong S.B., Kim M.S., 2017. Refrigerant leakage detection in an EEV installed residential air conditioner with limited sensor installations. Int. J. Refrig. 78, 157-165.

Yoon, P., Kang, D., Kim, C., Ahn, S., Chung, B., Kim, B., Lee, J., Hwang, Y., 2011. An experimental study on oil discharge ratio at inverter-driven high shell pressure scroll compressor using R410A/PVE. Int. J. Refrig. 34, 105-112.

Youbi-Idrissi, M., Bonjour, J., 2008. The effect of oil in refrigeration: Current research issues and critical review of thermodynamic aspects. Int. J. Refrig. 31, 165-179.

Zivi, S., 1964. Estimation of Steady-state Steam Void-fraction by Means of the Principle of Minimum Entropy Production. J. Heat Transfer. 86, 247-251.

국 문 초 록

본 연구에서는 공기 열펌프 시스템의 냉매 누설량에 대한 두 가지 검출 방법을 제안하고 모델링 및 실험을 통해 검증하였다. 냉매 누설은 열펌프에서 고장에서 가장 큰 빈도 및 비용을 차지하는 고장으로 누설량을 판단하는 것은 중요하다. 누설이 발생하면 먼저 누설 지점을 찾아야 하는데 이는 적절한 누설 감지기가 있으면 비교적 쉽다. 그 후 시스템에서 유출된 냉매량 만큼을 다시 채워야 하는데 냉매량을 판단하기 위해서는 시스템의 특성을 이용하여야 한다.

열펌프 시스템의 모델링에서는 윤활유와 냉매의 혼합물 특성이 반영되어야 하는데 이유는 윤활유를 고려하지 않은 모델이 냉매량을 실제값보다 약 10~30% 적은 값으로 예측하기 때문이다. 냉매는 액체 상태로 윤활유에 용해되어 있기 때문에 그 양을 무시할 수 없다. 이 때문에 냉매와 윤활유의 혼합물 특성을 반영한 모델링을 통해서 냉매량을 실제값과 근사하게 예측할 수 있다.

가정용 및 상업용 공기열원 열펌프를 대상으로 하여 모델링 및 실험을 통해 냉매누설량 탐지방법이 각각 제안되었다. 가정용 시스템은 측정변수가 적기 때문에 제한된 정보 내에서 현재 냉매량을 찾아야한다. 본 연구에서 제안된 방법은 실내 공기 입구와 증발기 중간 지점에 위치한 두 개의 온도 센서 값의 차이를 이용하는 방법이다. 정상 충전 조건에서는 증발기 중간 지점이 2상 상태로 존재하기 때문에 두 온도값 차이가 크지만 누출 된 상태에서 증발기 중간 지점의 상태가 과열상태로 진입하면서 온도가 상승하여 실내공기 입구와의 온도차이가 작아진다. 이 방법을 이용하면, 충전수준 55 ~ 65%에서 냉매누설을 판정할 수 있다. 하지만 실제로는 더 높은 충전수준에서 판단하는 것이 바람직하며 앞선 방법에 더하여 EEV의 개도를 의도적으로 줄이는 제어 방법을 사용하면 냉매량을 판단하는 충전수준의 범위를 80%까지 증가시킬 수 있다.

상업용 열펌프 시스템의 냉매량 판단을 위해 제안된 방법은 로그

평균 온도차를 이용한 방법이다. 이는 과열도가 일정하게 유지될 때 충전수준과 응축압력 사이의 관계가 선형적임을 이용한 것으로 다양한 온도조건과 압축기 회전 속도조건을 고려하더라도 시스템의 현재 충전량을 5.9%의 오차로 예측할 수 있다. 본 연구는 공기 열펌프 시스템의 충전량 판단을 위해 유용하게 쓰일 수 있고 제안된 방법은 기존 시스템에 즉시 적용될 수 있다.

주요어: 공기열원 열펌프, 냉매 윤활유 혼합물, 냉매충전량, 냉매누설탐지

학 번: 2012-22555